Inorganic Chemistry

Article

pubs.acs.org/IC

Bioinspired Nonheme Iron Complexes Derived from an Extended Series of N,N,O-Ligated BAIP Ligands

Marcel A. H. Moelands,[†] Sjoerd Nijsse,[†] Emma Folkertsma,[†] Bas de Bruin,[‡] Martin Lutz,[‡,§] Anthony L. Spek,[‡,§] and Robertus J. M. Klein Gebbink*[,†]

[†]Organic Chemistry and Catalysis, Debye Institute for Nanomaterials Science, Faculty of Science, Utrecht University, Universiteitsweg 99, 3584 CG Utrecht, The Netherlands

[‡]Van't Hoff Institute for Molecular Sciences (HIMS), University of Amsterdam, P.O. Box 94720, 1090 GE Amsterdam, The Netherlands

[§]Bijvoet Center for Biomolecular Research, Crystal and Structural Chemistry, Faculty of Science, Utrecht University, Padualaan 8, 3584 CH Utrecht, The Netherlands

Supporting Information

ABSTRACT: A series of mononuclear Fe(II) triflate complexes based on the 3,3-bis(1-alkylimidazole-2-yl)propionate ester (**BAIP**) ligand scaffold are reported. In these complexes, the tripodal N,N,O-**BAIP** ester ligand is varied by (i) changing the ester moiety (i.e., *n*-Pr, *tert*-Bu esters, *n*-Pr amide), (ii) changing the methylimidazole moieties to methylbenzimidazole moieties, and (iii) changing the methylimidazole moieties to 1-ethyl-4-isopropylimidazole moieties. The general structure of the resulting complexes comprises two facially capping **BAIP** ligands around a coordinatively saturated octahedral Fe(II) center, with either a transoid or cisoid orientation of the N,N,O-donor manifold that depends on the combined steric and electronic demand of the ligands. In the case of the sterically most encumbered ligand, a four-coordinate all N-coordinate complex is formed as well, which cocrystallizes with the six-coordinate complex. In combination with the catalytic properties of the new complexes in the epoxidation/cis-dihydroxylation of cyclooctene with H_2O_2, in terms of turnover number and cis-diol formation, these studies provide a number of insights for further ligand design and catalyst development aimed at Fe-mediated cis-dihydroxylation.

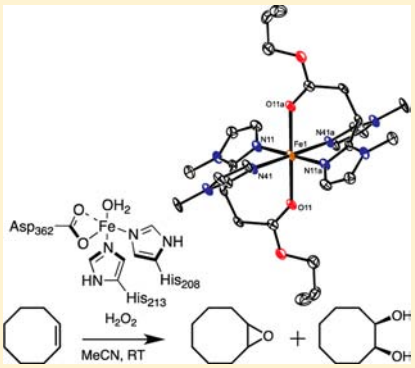

INTRODUCTION

Oxidation reactions are important in the production of bulk and fine chemicals. More than 20% of all organic products made in the chemical industry are obtained via catalytic oxidation reactions.[1] The catalysts used in these reactions have an additional role when the stereochemistry of the oxidation product is of interest, for instance, in the production of building blocks for the pharmaceutical industry. Of particular interest in this respect are catalysts that are able to bring about the stereoselective cis-dihydroxylation of alkenes to their corresponding vicinal diols.

Several procedures are known to oxidize selectively alkene substrates to their corresponding cis-diols, but in most cases these reactions are associated with several unwanted drawbacks or problems.[2] For example, osmium tetraoxide can be used catalytically in the presence of a secondary oxidant (e.g., hydrogen peroxide) to facilitate alkene cis-dihydroxylation.[3] The Sharpless AD-mixes α and β are commercially available osmium-based reagent mixtures for the asymmetric dihydroxylation of alkenes.[4] Although these systems are very reliable, the obvious disadvantages of the use of osmium are its price and toxicity. Several examples of alkene cis-dihydroxylation using ruthenium as an alternative to osmium have been reported.[5−7] Unfortunately, these ruthenium systems are not as selective as the osmium ones, and ruthenium is considered to be an expensive metal. Alternatively, $KMnO_4$ may be used for alkene cis-dihydroxylation, although stoichiometric amounts of this oxidant have to be used.[8,9] Catalytic systems based on manganese have been reported by Feringa[10] and Che.[11]

The answer to finding a good alternative to osmium in cis-dihydroxylation reactions might be found in nature, where several classes of metalloenzymes catalyze a wide variety of oxidation reactions. Rieske oxygenases are one important class of enzymes from the perspective of cis-dihydroxylations.[12] These dioxygenases are found in soil bacteria and catalyze the first step in the biodegradation of aromatic compounds by performing a cis-dihydroxylation on the arene substrate.[13] Because this reaction is regio- and stereospecific, it was investigated extensively over the past two decades, resulting in a range of crystallographic and mechanistic studies. The enzyme that has been most studied is naphthalene dioxygenase (NDO), which catalyzes the cis-dihydroxylation of naphthalene to *cis*-(1*R*,2*S*)-1,2-dihydronaphtalene-1,2-diol. The combined crystal-

Received: January 14, 2013
Published: June 10, 2013

   dx.doi.org/10.1021/ic400096e | *Inorg. Chem.* 2013, 52, 7394−7410

lographic data on Rieske dioxygenases show that the catalytic sites of these dioxygenases are very similar. Each consists of a mononuclear iron center anchored to the enzyme by two histidine residues and a mono- or bidentate carboxylate ligand from either an aspartate or a glutamate residue (Figure 1).

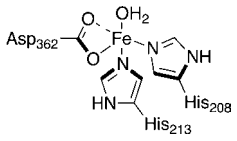

Figure 1. Structure of the monoiron(II) active site in naphthalene 1,2-dioxygenase.

Depending on the coordination mode of the carboxylate, this active-site architecture is referred to as either the 2-His-1-carboxylate facial triad (monodentate carboxylate)[14] or the 2-His-1-carboxylate structural motif (bidentate carboxylate binding).[12] Because iron adopts an octahedral geometry in these enzymes, there are respectively three or two vacant sites left to bind the substrate, dioxygen, and/or cofactor ligands. If none of these are bound, then the sites are either occupied by weakly bonded solvent molecules or are vacant.

Interest in the catalytic properties of the Rieske dioxygenase has led to several endeavors that are trying to grasp its structure and reactivity in synthetic model systems. The structure of the 2-His-1-carboxylate facial triad structural motif has, in addition, become a designer platform for the development of synthetic Fe-based dihydroxylation catalysts. The group of Que and coworkers was the first to synthesize a successful catalyst based on the active site of NDO.[15] Compound $[Fe(II)(6\text{-}Me_3\text{-}tpa)(CH_3CN)_2](ClO_4)_2$ (6-Me_3-tpa = tris[(6-methylpyridin-2-yl)methyl]amine) is able to convert a number of aliphatic alkenes to their corresponding cis-diol products (in combination with some epoxide byproducts) with the use of hydrogen peroxide as the oxidant. As a critical structural feature, the Fe(6-Me_3-tpa) complex contains two labile cis-coordination sites that are occupied by CH_3CN molecules. Que and co-workers later reported on the synthesis of the chiral Fe(II) complex [Fe(6-Me-BPBP)$(OTf)_2$] (BPBP = bis(pyridinylmethyl)-bipyrrolidine) that is able to form cis-diols from olefins in up to 97% ee.[17] These systems are currently the most selective iron-based catalysts for the dihydroxylation of olefins. Other Fe-based systems able to carry out cis-dihydroxylations include systems based on bispidine and on (bi)cyclic tetraaza ligands.[18]

A typical feature of the above systems is that they all contain an all-nitrogen-ligand donor set, instead of the mixed N,O donor set found in the Rieske dioxygenases. In addition, these systems do not follow the facially capping tridentate-designer mold laid down by the 2-His-1-carboxylate facial triad. In 2005, Que and co-workers reported on the Ph-DPAH ligand (DPAH = di(2-pyridyl)methylbenzamide) that has an N,N,O donor set.[16] Corresponding iron complex $[Fe(II)(Ph\text{-}DPAH)_2](OTf)_2$ has an octahedral geometry in which the two carbonyl oxygen donors are trans to each other. Although this iron complex is coordinatively saturated, it does catalyze the oxidation of olefins. During these reactions, one ligand most likely dissociates from the iron center to make three sites available for substrate and hydrogen peroxide binding. The complex forms the cis-diol as the major product for a range of olefins, with conversions of 50−80% depending on the amount of hydrogen peroxide added, and does so with a retention of the olefin configuration.

Along a similar vein, other N,N,O ligands are currently being explored to mimic the structural aspects of the 2-His-1-carboxylate facial triad more accurately. Examples of ligands that are used in these studies in combination with iron include the scorpionate-type bis(pyrazol-1-yl) acetates[19] and mixed proline−pyridine ligands.[20] Iron complexes of bispyrazolyl acetate ligands were quite extensively studied by Burzlaff and coworkers,[19c] whereas more recently, Jones et al. have developed some sterically encumbered versions of these ligands.[21]

In recent articles, we have reported on the syntheses of iron(II) complexes derived from a new class of facial N,N,O ligands.[22−24] The tripodal 3,3-bis(1-alkylimidazole-2-yl)-propionate (**BAIP**) ligands contain two imidazole groups and a carboxylate moiety to mimic the histidine and aspartate residues in the active site of NDO (Figure 2). These anionic N,N,O ligands form mononuclear iron complexes in the presence of an additional anionic ligand, for instance, catecholate. In the absence of such additional ligands, coordinatively saturated [Fe(**BAIP**)$_2$] complexes are formed that were found to be inactive as oxidation catalysts.[23] Changing the carboxylate into a carboxylate ester changes the coordination properties of these ligands. Depending on the counterion and the solvent that are used, either a trans bis-ligand complex or bis-solvent bis-ligand adduct is formed (Figure 2). In the latter adduct, the **BMIP^{nPr}** ligands (**BMIP^{nPr}** = propyl 3,3-bis(1-methylimidazole-2-yl)propionate) act as N,N donors and two MeOH molecules coordinate to iron in

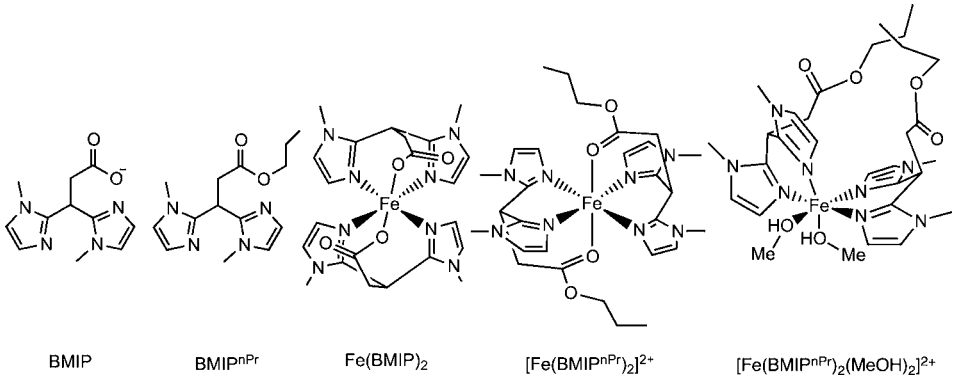

Figure 2. Ligands 3,3-bis(1-methylimidazole-2-yl)propionate (**BMIP**) and propyl 3,3-bis(1-methylimidazole-2-yl)propionate (**BMIP^{nPr}**) and some of their iron(II) complexes.

dx.doi.org/10.1021/ic400096e | Inorg. Chem. 2013, 52, 7394−7410

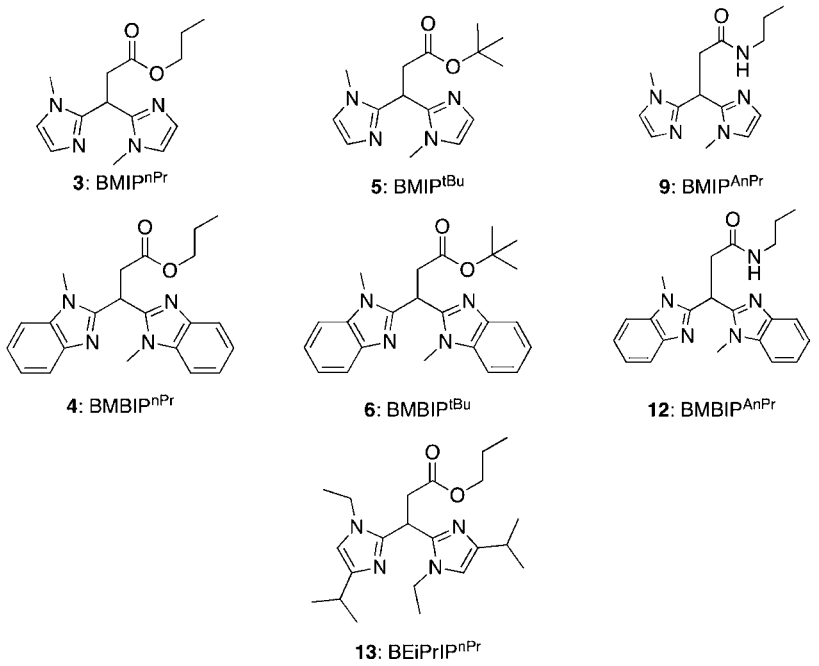

Figure 3. Overview of **BAIP**-type ligands.

Scheme 1. Synthesis of Ligands 3–6[a]

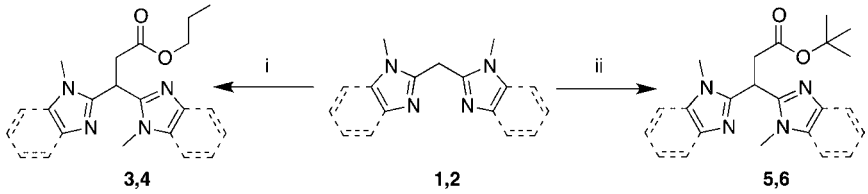

[a] (i) (a) *n*-BuLi, THF, −78 °C, 1 h; (b) propyl bromoacetate, −78 °C to rt, overnight. (ii) (a) *n*-BuLi, THF, −78 °C, 1 h; (b) *tert*-butyl bromoacetate, −78 °C to rt, overnight.

Scheme 2. Synthesis of Amide Ligands 9 and 12[a]

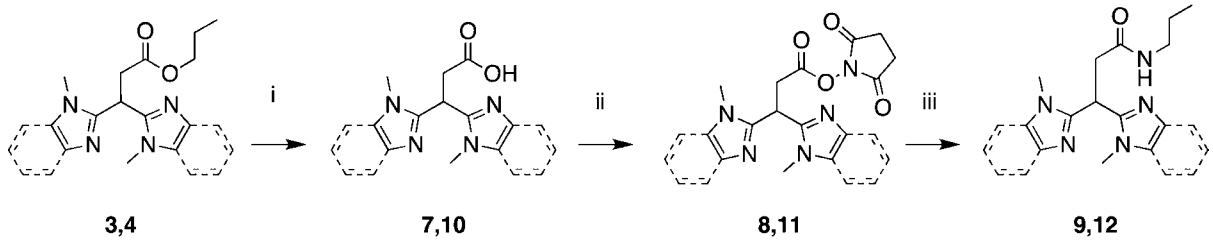

[a](i) (a) One equiv KOH, THF, rt; (b) one equiv HCl. (ii) NHS, DCC, pyridine, THF, 35–40 °C . (iii) Propylamine, CH_2Cl_2, rt.

a cis fashion. When the trans bis-ligand complex [Fe(**BMIP**^{nPr})$_2$](OTf)$_2$ is used in the oxidation of alkenes with H_2O_2, in addition to the formation of the epoxide product, the formation of the cis-diol product is also observed.[23] The formation of the cis-diol products indicates the flexibility of the ligand system because for the cis-diol product to be formed two-labile cis sites are deemed necessary on the metal center. The [Fe(**BMIP**^{nPr})$_2$](OTf)$_2$ complex most likely rearranges in solution to a structure that is similar to that observed for the MeOH adduct.

Here, we report on an extension of this work by the synthesis of several analogues of the **BMIP**^{nPr} ligand in the search for more selective cis-dihydroxylation catalysts based on iron. A number of different ligands were investigated, which can be divided into three different groups (Figure 3). In the first group, the two 1-methylimidazole donors of the **BMIP** structure were combined with different ester or amide donors. In the second group, the 1-methylimidazole donors were substituted for 1-methylbenzimidazole donors to induce more steric bulk around the nitrogen donors and to make the ligand more soluble in apolar solvents. In the third group, the 1-methylimidazole donors of the ligand were replaced with 1-ethyl-4-isopropylimidazole donors. The coordination behavior of these N,N,O ligands toward iron and the catalytic behavior of the resulting complexes in the oxidation of cyclooctene were investigated.

dx.doi.org/10.1021/ic400096e | *Inorg. Chem.* 2013, 52, 7394–7410

Scheme 3. Synthesis of Iron Triflate Complexes 14−20 (Generalized Structure Shown)

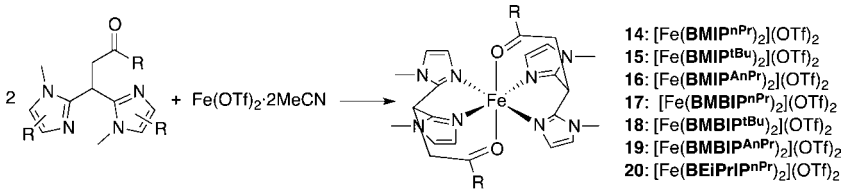

RESULTS AND DISCUSSION

Ligand Synthesis. Ligands **BMIP^{nPr}** (**3**) and **BMBIP^{nPr}** (**4**) were synthesized according to a synthesis route previously reported by our group[25] that was also employed for the synthesis of ligands **BMIP^{tBu}** (**5**) and **BMBIP^{tBu}** (**6**) (Scheme 1). The starting bis(1-methylimidazole-2-yl)methane (**1**)[26,27] and bis(1-methylbenzimidazole-2-yl)methane (**2**)[28] compounds can be easily synthesized on a multigram scale. Lithiation of these bis(imidazole)methanes at the methylene position using *n*-BuLi at −78 °C followed by the addition of either *n*-propylbromoacetate or *tert*-butylbromoacetate yielded propyl 3,3-bis(1-methylimidazole-2-yl)propionate, **BMIP^{nPr}** (**3**), propyl 3,3-bis(1-methylbenzimidazole-2-yl)propionate, **BMBIP^{nPr}** (**4**), *tert*-butyl 3,3-bis(1-methylimidazole-2-yl)-propionate, **BMIP^{tBu}** (**5**), and *tert*-butyl 3,3-bis(1-methylbenzimidazole-2-yl)propionate, **BMBIP^{tBu}** (**6**), respectively, in good yields (83−94%).

The preparation of the amide-appended ligands 3,3-bis(1-methylimidazol-2-yl)-*N*-propylpropanamide, **BMIP^{AnPr}** (**9**), and 3,3-bis(1-methylbenzimidazol-2-yl)-*N*-propylpropanamide, **BMBIP^{AnPr}** (**12**), proceeded via the preparation of an active ester intermediate (Scheme 2). First, propyl ester ligands **3** and **4** were hydrolyzed using 1 equiv of KOH.[25] The resulting carboxylic acids were turned into active esters by DCC coupling according to a modified procedure by Suijkerbuijk et al.[29] The yield of **8** (43%) was much lower in comparison to the yield of **11** (85%), which was caused by the low solubility of acid **7** in THF. In the final step, the active esters were reacted with propylamine to yield the desired amide ligands **9** and **12** in 25 and 90% isolated yields after recrystallization, respectively. The preparation of the **BEiPrIP^{nPr}** ligand (**13**) with two 1-ethyl-4-isopropylimidazole donors was previously reported by us.[30]

Fe Triflate Complexes. For the set of seven ligands, the corresponding iron bis-ligand complexes were synthesized in the same way as was reported for the **BMIP^{nPr}** complex (Scheme 3).[23] For the preparation of the complexes, the appropriate ligand was mixed in a 2:1 ratio with Fe(OTf)$_2$·2MeCN[31] in methanol for 1 h. After the solvent was removed, recrystallization of the resulting brown or (off) white powders from an acetonitrile/diethyl ether mixture yielded iron complexes [Fe(**BMIP^{nPr}**)$_2$](OTf)$_2$ (**14**),[23] [Fe(**BMIP^{tBu}**)$_2$](OTf)$_2$ (**15**), [Fe(**BMBIP^{nPr}**)$_2$](OTf)$_2$ (**17**), [Fe(**BMBIP^{tBu}**)$_2$](OTf)$_2$ (**18**), [Fe(**BMBIP^{AnPr}**)$_2$](OTf)$_2$ (**19**), and [Fe(**BEiPrIP^{nPr}**)$_2$](OTf)$_2$ (**20**) as crystalline solids in high yields (79−95%); however, the yield of **20** was much lower (34%) because of the two consecutive crystallization steps in its purification. Corresponding iron bis-ligand complex **16**, derived from ligand **BMIP^{AnPr}**, was not synthesized as isolated material but was instead prepared in situ for catalytic testing.

These paramagnetic complexes were characterized by different techniques, including single-crystal X-ray structure determination, IR spectroscopy, and ESI-MS analysis. All prepared complexes were stored as dry powders under a nitrogen atmosphere. Benzimidazole amide complex **19** proved quite sensitive toward oxidation, even under these storage conditions. The color of the dry powder of **19** turned red overnight, indicating the oxidation of Fe(II) to Fe(III) in this complex.

High-resolution mass spectroscopy analysis (ESI-MS) proved very conclusive in the composition of the isolated materials. In all cases, monocations of the composition [Fe(L$_2$)(OTf)]$^+$ were recorded as the parent peak. This composition is in agreement with the anticipated composition of the complexes as [Fe(L$_2$)](OTf)$_2$ on the basis of the first-generation complex [Fe(**BMIP^{nPr}**)$_2$](OTf)$_2$.[23]

IR spectra were recorded for the different complexes, both in the solid state and in solution. The IR spectrum of [Fe(**BMIP^{nPr}**)$_2$](OTf)$_2$ (**14**) in the solid state showed a clear vibrational band of the carbonyl group at 1691 cm^{-1}, whereas the frequency of the carbonyl vibration in the free ligand was found at 1727 cm^{-1}. This frequency shift indicates the coordination of the carbonyl group to the iron center. The symmetric and asymmetric vibrations of the CF_3 and SO_3 groups of the triflate anions in [Fe(**BMIP^{nPr}**)$_2$](OTf)$_2$ were found at 1259 (ν_{as} SO_3), 1216 (ν_s CF_3), 1152 (ν_{as} CF_3), and 1030 (ν_s SO_3) cm^{-1}, which indicates that these are noncoordinating ions.[32] Similar observations were made in the solid state for complexes **15**, **18**, and **19**, pointing to solid-state structures that are similar that of **14** (Table 1).

Table 1. Solid-State IR Vibrations of Complexes 14, 15, 18, and 19

complex	ligand ν(C=O)(cm^{-1})	complex ν(C=O)(cm^{-1})	triflate vibrations ν(cm^{-1})
[Fe(**BMIP^{nPr}**)$_2$](OTf)$_2$ (**14**)	1727	1691	1259, 1216, 1152, 1030
[Fe(**BMIP^{tBu}**)$_2$](OTf)$_2$ (**15**)	1726	1692	1258, 1224, 1144, 1029
[Fe(**BMBIP^{tBu}**)$_2$](OTf)$_2$ (**18**)	1720	1665	1260, 1226, 1150, 1030
[Fe(**BMBIP^{AnPr}**)$_2$](OTf)$_2$ (**19**)	1656	1628	1244, 1223, 1151, 1028

In the case of benzimidazole complex [Fe(**BMBIP^{nPr}**)$_2$](OTf)$_2$ (**17**), two carbonyl-stretching vibrations were found: a strong vibration at 1694 cm^{-1} and a shoulder at 1709 cm^{-1} that both point to coordinating carbonyl groups (free ligand at 1734 cm^{-1}). It is likely that both the cis and trans isomers of the complex are present in the solid state. For [Fe(**BEiPrIP^{nPr}**)$_2$](OTf)$_2$ (**20**), several carbonyl-stretching vibrations were observed. Just as in **17**, two bands that correspond to coordinating carbonyl groups were found (1705, 1691 cm^{-1}), again implying the presence of both cis and trans isomers. In addition, a strong vibration was found for a noncoordinating carbonyl moiety at 1736 cm^{-1} (free ligand 1734 cm^{-1}). This

dx.doi.org/10.1021/ic400096e | Inorg. Chem. 2013, 52, 7394−7410

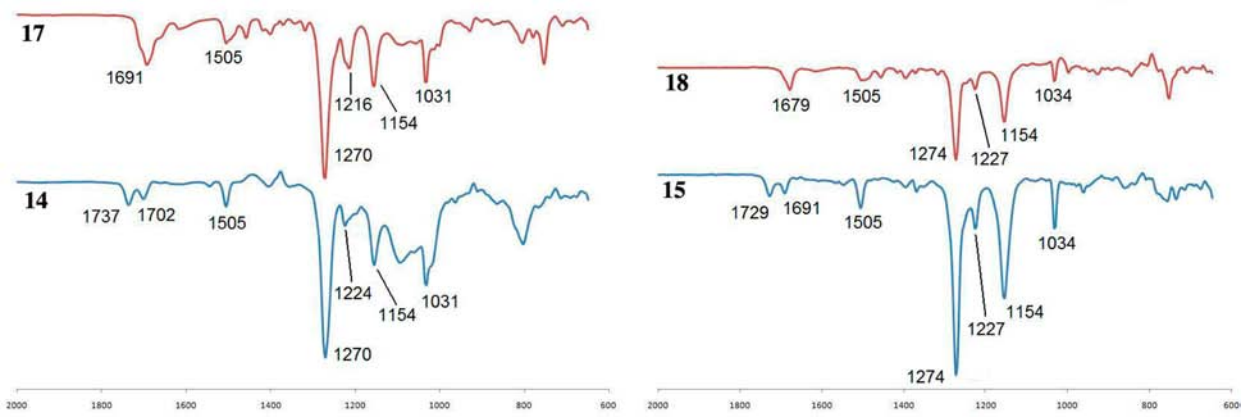

Figure 4. Solution IR spectra of complexes **14** and **17** (left) and **15** and **18** (right) in acetonitrile. Vibrational energies are given in wavenumbers (cm^{-1}).

indicates that at least three different forms of the complex are present in the solid state. On the basis of these IR data, the triflate groups do not coordinate to iron in the solid state in complexes **17** and **20**.

For several of the complexes, solution IR spectra were recorded in acetonitrile. In previous work on complex **14**, it was found that in solution some of the carbonyl oxygens detach from the iron center to create a vacant site[23] to which either a triflate ion or a solvent molecule could coordinate. For $[Fe(\mathbf{BMIP^{nPr}})_2](OTf)_2$ (**14**), two distinct C=O stretching vibrations were observed: one at 1737 cm^{-1} (noncoordinated) and one at 1702 cm^{-1} (coordinated; Figure 4). When the imidazole donors were substituted for benzimidazole donors as in $[Fe(\mathbf{BMBIP^{nPr}})_2](OTf)_2$ (**17**), only one C=O vibration corresponding to a coordinated carbonyl group was present at 1691 cm^{-1}. However, this intense peak has small shoulders, indicating the possible presence of other species in solution.

For $[Fe(\mathbf{BMIP^{tBu}})_2](OTf)_2$ (**15**) and corresponding benzimidazole compound $[Fe(\mathbf{BMBIP^{tBu}})_2](OTf)_2$ (**18**), similar IR features were observed in acetonitrile (Figure 4, right). Compound **15** again showed two distinct carbonyl peaks, and compound **18** showed one sharp carbonyl peak. These observations indicate that the presence of the benzimidazole group hinders/prevents the decoordination of the carbonyl groups in solution. Figure 4 also shows the triflate vibrations for the four complexes in the 1000−1300 cm^{-1} region. These vibrations are characteristic of noncoordinated triflates.[32] Because of the low-yielding synthesis of the amide ligands, no solution IR spectrum could be obtained for the corresponding Fe compounds.

Structural Features of the Iron Triflate Complexes in the Solid State (X-ray Crystal Structures). Crystals of complexes **14**−**20** suitable for X-ray analysis were obtained by slow vapor diffusion of diethyl ether into a solution of the corresponding complex in acetonitrile. The crystal structures for the first group of complexes with the imidazole backbone, $[Fe(\mathbf{BMIP^{nPr}})_2](OTf)_2$ (**14**), $[Fe(\mathbf{BMIP^{tBu}})_2](OTf)_2$ (**15**), and $[Fe(\mathbf{BMIP^{AnPr}})_2](OTf)_2$ (**16**), are depicted in Figure 5.

In the crystal structures of complexes **14**−**16**, the Fe atoms of all molecules are located on inversion centers. The complexes have a nearly ideal octahedral geometry. Both ligands in these complexes are coordinated in a facial manner around the iron center, with the two coordinating carbonyl groups in the trans position with respect to each other. The two ester complexes, **14** and **15**, are very much alike. Their ester moieties point away from the iron center and do not exert a noticeable effect on the coordination geometry around iron. Amide ligand $\mathbf{BMIP^{AnPr}}$ coordinates in the same way to iron as does the $\mathbf{BMIP^{nPr}}$ ligand (i.e., the amide moiety coordinates to iron via its carbonyl group, and the propyl amide tails point away from iron). Bruijnincx et al. have earlier reported on the structure of complex **14**.[23] In that case, the crystals were obtained from a $MeOH/Et_2O$ mixture, and a different structure was obtained $[Fe(\mathbf{BMIP^{nPr}})_2(MeOH)_2](OTf)_2$ in which the two ligands coordinate to iron via the nitrogen-donor atoms only and two molecules of MeOH are coordinated in a cis fashion to the iron center (Figure 2). A structure of the corresponding tetraphenylborate complex $[Fe(\mathbf{BMIMP^{nPr}})_2](BPh_4)_2$ was also reported.[23] In this case, the structure matches the structure of **14** reported here.

Table 2 shows selected bond lengths and angles for complexes **14**−**16**, and for each complex, the data for all independent residues in the asymmetric unit are shown. The observed Fe−N bond lengths vary between 2.105(3) and 2.147(6) Å and are characteristic of iron(II) high-spin complexes with imidazole-like ligands.[33,34] Overall, the variation of bond lengths in the individual complexes is very small, as can be seen in the quadratic elongation $\langle\lambda_{oct}\rangle$.[35] The intraligand N−Fe−N angles are all smaller than 90°, reflecting the small "bite angle" of the bis-imidazole methane moiety, whereas all interligand N−Fe−N angles are larger than 90°. All complexes have a significant angular variance σ_{oct}^2.[35] A comparison of all independent molecules in the crystal structures of **14**−**16** shows only minor differences in the bond lengths and angles. The variation in the ester moiety in the first group of **BMIP** ligands, therefore, does not have a large effect on the overall structure of the corresponding $[Fe(\mathbf{BAIP})_2](OTf)_2$ complexes.

The structures of the three complexes of the benzimidazole group $[Fe(\mathbf{BMBIP^{nPr}})_2](OTf)_2$ (**17**), $[Fe(\mathbf{BMBIP^{tBu}})_2](OTf)_2$ (**18**), and $[Fe(\mathbf{BMBIP^{AnPr}})_2](OTf)_2$ (**19**) are shown in Figure 6. In contrast to centrosymmetric complexes **14**−**16**, complex **17** is located on a 2-fold rotation axis with a cisoid coordination of the ligands. The basal plane of **17** is formed by symmetry-related nitrogen atoms N31 and N31*a* and oxygen atoms O21 and O21*a* ($a = x$, $0.5 - y$, $0.5 - z$). The symmetry-related nitrogen atoms N11 and N11*a* are above and below this plane, respectively. Both solid-state and solution-IR spectra of complex **17** indicate the presence of more than one species, which does not rule out the presence of an isomer of **17** in which the oxygen donors are in the trans position. Most likely,

dx.doi.org/10.1021/ic400096e | Inorg. Chem. 2013, 52, 7394−7410

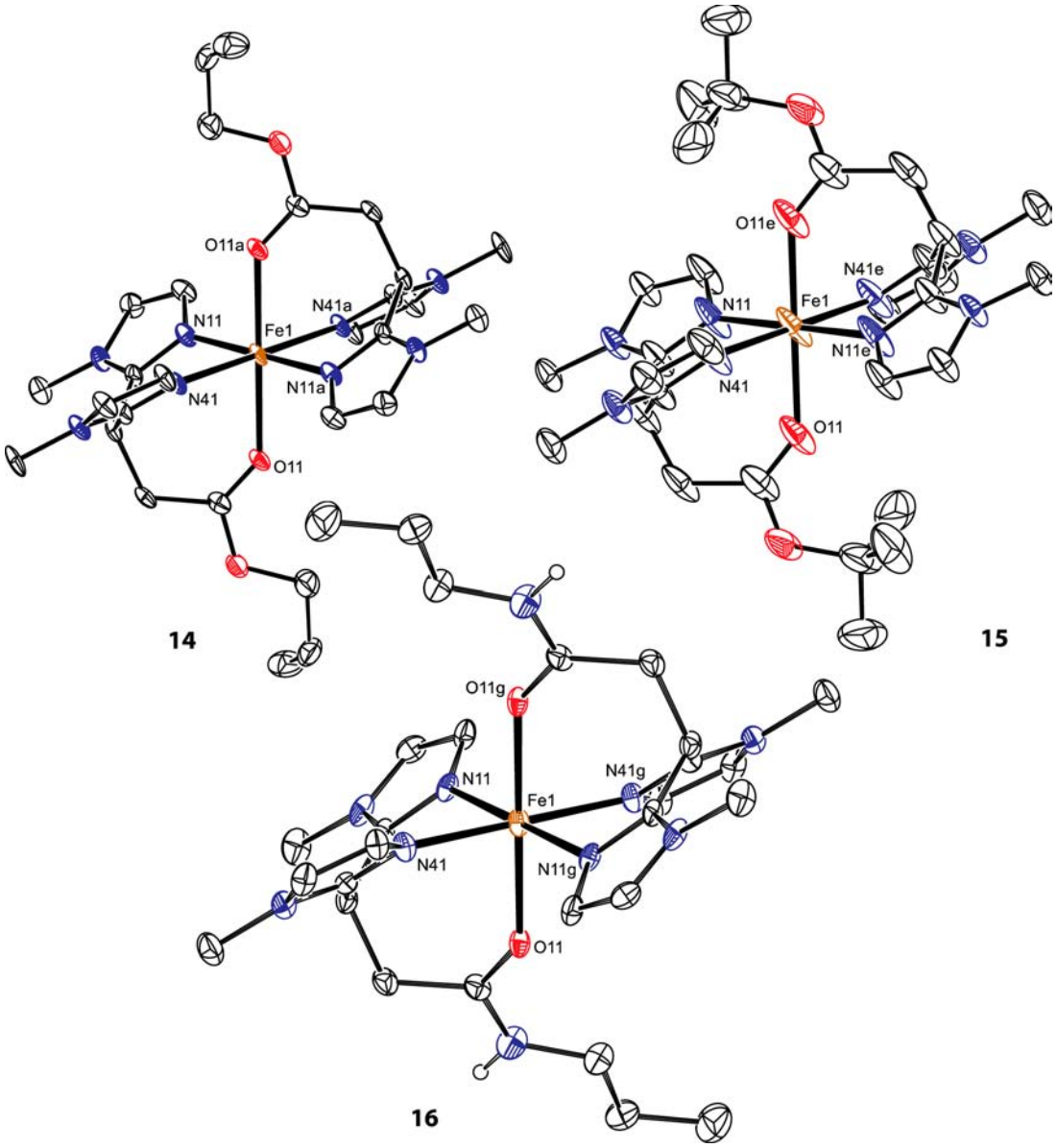

Figure 5. Molecular structures of cationic complexes **14**–**16** in the crystals shown with displacement ellipsoid plots (30% probability). All C–H hydrogen atoms, noncoordinated triflate anions, and noncoordinated acetonitrile molecules are omitted for clarity. In **14**, only one out of four independent molecules is shown, and only the major conformation of the disordered *n*-propyl moiety is displayed. In **15**, only one out of two independent molecules is depicted. Symmetry operations: (a) $-x, -y, -z$; (e) $1-x, -y, 1-z$; (g) $1-x, 1-y, 1-z$.

the cis isomer crystallizes preferentially. This different coordination behavior of benzimidazole complex **17** in comparison to its imidazole derivative **14** might be caused by the presence of the more bulky benzimidazole groups that preclude the formation of a single thermodynamic conformer. However, the structure of [Cu(**BMBIP**)$_2$], containing the analogous anionic benzimidazole propionate ligand, was earlier found to crystallize in a transoid manner,[25] which may indicate an additional role for the ester moiety in determining the overall structure.

Complexes **18** and **19** show the same coordination geometry as that of complexes **14**–**16**, a distorted octahedral coordination with the carbonyl oxygens in the trans position. Although complex **19** is again centrosymmetric, complex **18** is located in a general position and has no molecular symmetry. Nevertheless, the distortion of the octahedral geometry in **18** is only slightly larger than that of the other complexes. The N,N,O ligands in **18** are different from those in **17** in the sense that the *n*-propylester moieties in **17** are exchanged for *tert*-butyl ester moieties in **18**. In this case, the steric bulk of these *tert*-butyl groups seem to "suppress" or "overrule" the steric effect of the benzimidazole groups. A cis orientation of the *tert*-butyl ester groups most likely is unfavorable because of the steric congestion of these groups in this orientation. The introduction of an *n*-propyl amide group into **BMBIP^{AnPr}** also results in a trans-octahedral complex (**19**). In this case, steric reasons are less likely to be at play because the *n*-propyl ester moiety in **BMBIP^{nPr}** allowed the formation of cis complexes. It therefore seems more reasonable that electronic effects result in the trans disposition of the amide-oxygen donors. The amides are stronger donors than the esters and seem to overrule steric arguments (vide infra). Selected bond lengths and angles for complexes **17**–**19** are shown in Table 3.

dx.doi.org/10.1021/ic400096e | *Inorg. Chem.* 2013, 52, 7394–7410

Table 2. Selected Bond Lengths (Angstroms) and Angles (Degrees) for Complexes 14−16[a]

	14				15		16
	Res 1 ($x = 1, y = a$)	Res 2 ($x = 2, y = b$)	Res 3 ($x = 3, y = c$)	Res 4 ($x = 4, y = d$)	Res 1 ($x = 1, y = e$)	Res 2 ($x = 2, y = f$)	Res 1 ($x = 1, y = g$)
				Bond Lengths			
Fex−N1x	2.123(5)	2.144(5)	2.126(5)	2.130(5)	2.115(4)	2.140(3)	2.147(6)
Fex−N4x	2.124(4)	2.124(5)	2.136(5)	2.127(5)	2.137(4)	2.105(3)	2.107(7)
Fex−O1x	2.249(4)	2.174(4)	2.186(4)	2.229(4)	2.145(4)	2.167(3)	2.157(5)
$\langle\lambda_{oct}\rangle^b$	1.006	1.004	1.004	1.005	1.005	1.006	1.005
				Bond Angles			
N1x−Fex−N4x	85.35(18)	85.78(19)	85.31(19)	85.21(18)	85.14(14)	84.66(10)	83.9(2)
N1x−Fex−O1x	87.26(17)	85.88(17)	88.82(17)	86.37(16)	86.85(14)	85.12(10)	86.6(2)
N1x−Fex−N4xy	94.63(18)	94.22(19)	94.69(19)	94.79(18)	94.86(14)	95.34(10)	96.1(2)
N1x−Fex−O1xy	92.74(17)	94.12(17)	91.18(17)	93.63(16)	93.15(14)	94.88(10)	93.4(2)
N4x−Fex−O1x	86.33(16)	89.43(17)	85.89(17)	87.49(17)	85.46(16)	86.99(10)	89.5(2)
N4x−Fex−O1xy	93.67(16)	90.56(17)	94.11(17)	92.51(17)	94.54(16)	93.01(10)	90.5(2)
σ_{oct}^2 (deg^2)[c]	15.43	12.59	14.68	15.57	19.80	22.43	17.76

[a]Symmetry operations: (a) $-x, -y, -z$; (b) $-x, 1-y, -z$; (c) $1-x, -y, 1-z$; (d) $1-x, 1-y, -z$; (e) $1-x, -y, 1-z$; (f) $-x, -y, 1-z$; (g) $1-x, 1-y, 1-z$. [b]$\langle\lambda_{oct}\rangle = \Sigma_{i=1}^{6}(l_i/l_o)^2/6$ [c]$\sigma_{oct}^2 = \Sigma_{i=1}^{12}(\theta_i-90°)^2/11$

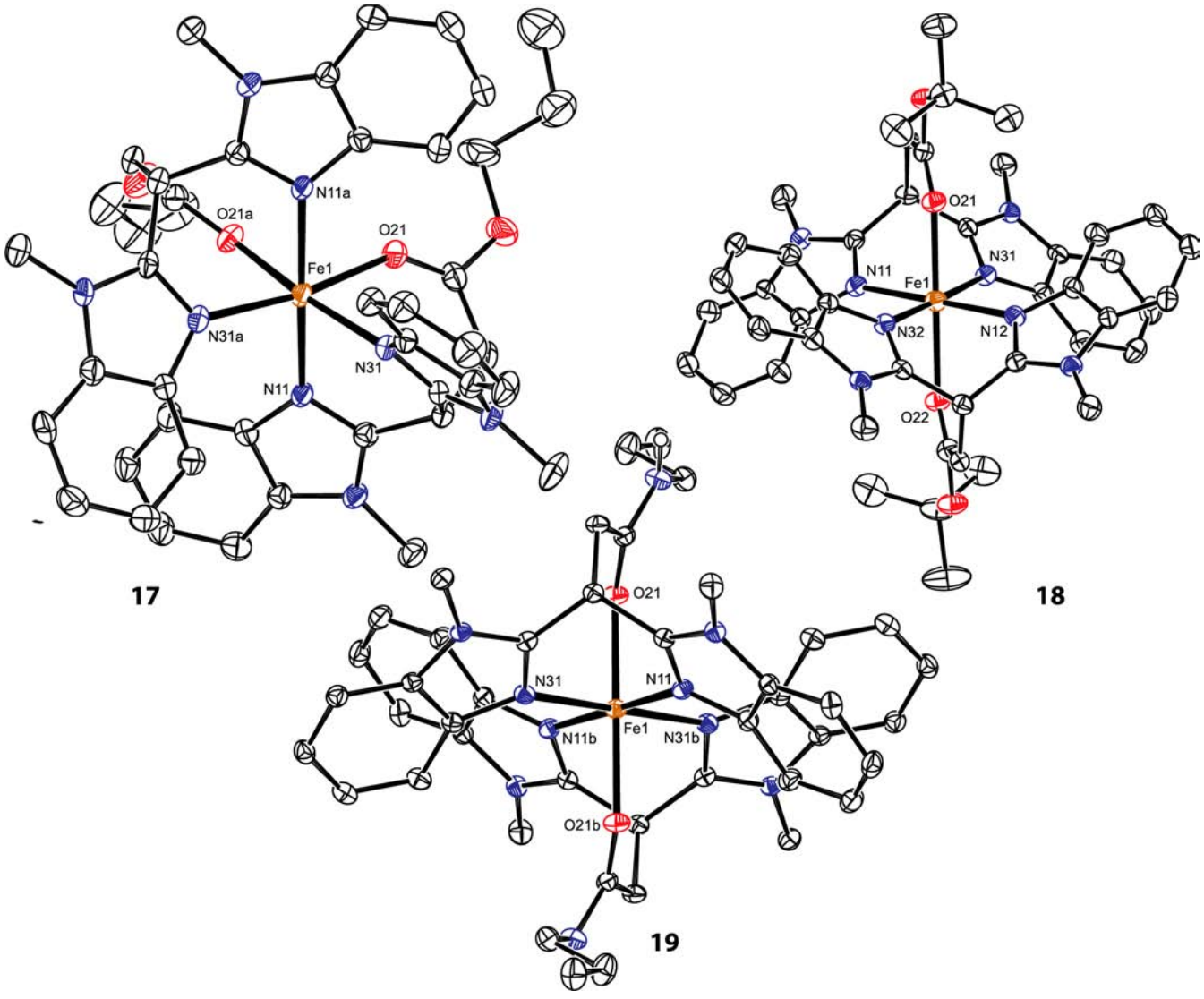

Figure 6. Molecular structures of the cations of complexes **17**−**19** in the crystals are shown with displacement ellipsoid plots (30% probability). All C−H hydrogen atoms, noncoordinated triflate anions, and noncoordinated acetonitrile molecules are omitted for clarity. Symmetry operations: (a) $x, 0.5-y, 0.5-z$; (b) $1-x, 1-y, 1-z$.

dx.doi.org/10.1021/ic400096e | Inorg. Chem. 2013, 52, 7394−7410

Table 3. Selected Bond Lengths (Angstroms) and Angles (Degrees) for Complexes 17−19.[a]

Bond Lengths				
	17 (y = a)	**19** (y = b)		**18**
Fe1−N11	2.115(3)	2.1426(15)	Fe1−N11	2.140(4)
Fe1−N31	2.115(3)	2.1584(15)	Fe1−N31	2.128(4)
Fe1−O21	2.180(3)	2.0886(13)	Fe1−O21	2.195(3)
			Fe1−N12	2.132(4)
			Fe1−N32	2.122(4)
			Fe1−O22	2.203(3)
$\langle\lambda_{oct}\rangle$	1.010	1.004		1.005
Bond Angles				
	17 (y = a)	**19** (y = b)		**18**
N11−Fe1−N31	87.31(13)	83.99(6)	N11−Fe1−N31	83.54(15)
N11−Fe1−O21	86.22(12)	89.57(6)	N11−Fe1−O21	88.65(14)
N11−Fe1−N11y	173.91(19)	180	N11−Fe1−N32	95.51(15)
N11−Fe1−N31y	96.48(13)	96.01(6)	N12−Fe1−N31	96.49(15)
N11−Fe1−O21y	89.23(12)	90.43(6)	N12−Fe1−N32	84.47(15)
N31−Fe1−N31y	103.4(2)	180	N12−Fe1−O22	87.74(14)
N31−Fe1−O21	86.81(13)	89.54(6)	N31−Fe1−O21	87.24(14)
N31−Fe1−O21y	169.54(13)	90.46(6)	N32−Fe1−O22	87.58(14)
O21−Fe1−O21y	83.12(17)	180	O21−Fe1−O22	178.91(13)
			N11−Fe1−N12	179.68(17)
			N31−Fe1−N32	178.40(16)
σ_{oct}^2 (deg^2)	34.12	13.25		17.08

[a]Symmetry operations: (a) x, 0.5 − y, 0.5 − z; (b) 1 − x, 1 − y, 1 − z.

Very similar trends in bond lengths and angles are found for **17**−**19** as compared to those of the first group, complexes **14**−**16**. All bond lengths are in agreement with high-spin (S = 2) iron(II) complexes. As found for complexes **14**−**16**, the intraligand N−Fe−N angles in **17**−**19** are smaller than 90°, reflecting the small bite angle of the bis-benzimidazole methane moiety. In complex **19**, the Fe−O bond length is considerably shorter than those in **17** and **18**, which indeed suggests that the carbonyl oxygen atoms in this complex are more tightly bound to the iron center. This effect is reflected among the series of complexes reported here by the overall shorter Fe−O bond lengths for the amide complexes (2.0886(13) and 2.157(5) Å) compared to those of the ester complexes (2.145(4) and 2.249(4) Å).

[Fe(**BEiPrIP**^{nPr})$_2$](OTf)$_2$ (**20**) crystallizes in the non-centrosymmetric space group $P1$, with three independent metal complexes in the unit cell in which two have tetrahedral coordination geometry and one has octahedral geometry. Figure 7 shows both the structure of the octahedral residue and the structure of one of the tetrahedral residues. The structure of the octahedral residue is reminiscent of the structure of complex **17** (i.e., an overall octahedral coordination geometry in which the oxygen donor atoms are found in cisoid positions). The combined bond lengths and angles again show a deviation from the ideal octahedral geometry, most likely caused by the tripodal structure of the ligand (Table 4). The bond lengths are in agreement with a high-spin (S = 2) iron(II) complex. In this residue, all bond lengths around Fe are larger than those in **17**. In particular, the Fe−O bond lengths are remarkably longer than those in **17** (2.252(3) and 2.303(3) vs 2.180(3) Å, respectively). These elongated bonds most likely reflect the overall steric demand of the **BEIPrIP**^{nPr} ligand as compared to that of the parent **BMIP**^{nPr} and **BMBIP**^{nPr} ligands.

In the tetrahedral residues of **20**, the **BEIPrIP**^{nPr} ligands act as bidentate nitrogen ligands, whereas the propyl ester moieties do not coordinate to iron but rather point away from the metal center. Selected bond lengths and angles for the two tetrahedral

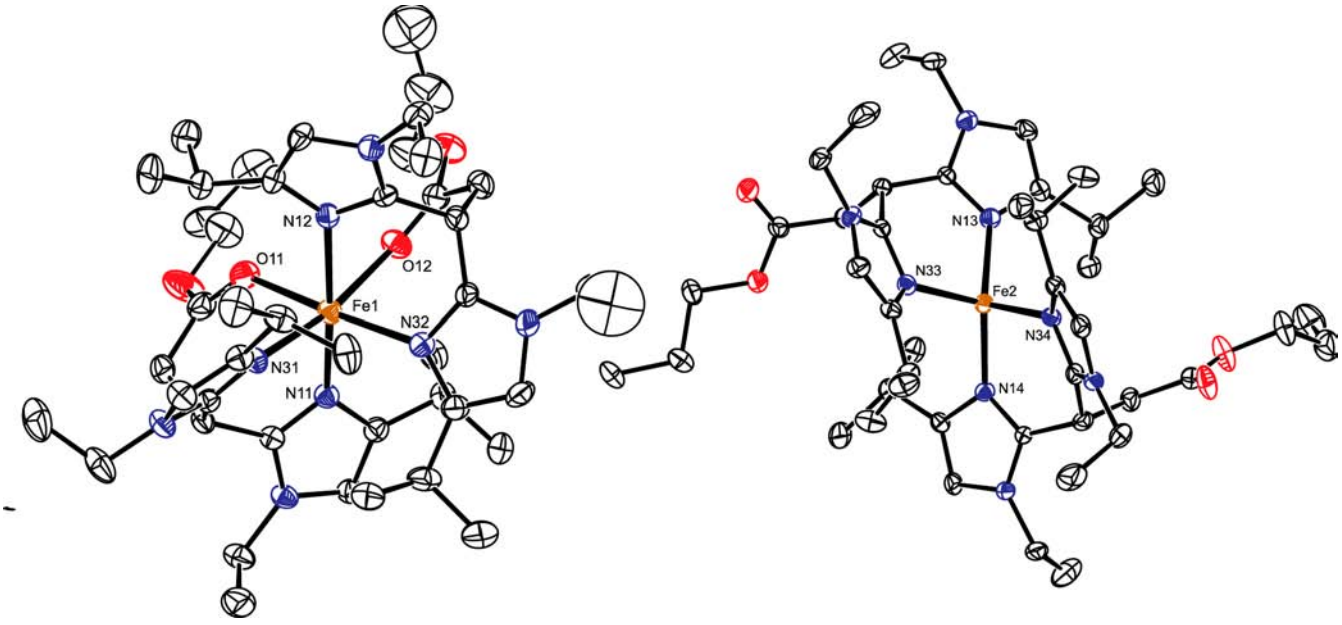

Figure 7. Molecular structures of the octahedral and the tetrahedral forms of the [Fe(**BEiPrIP**^{nPr})$_2$]$^{2+}$ cation in the crystal structure of **20** shown with displacement ellipsoid plots (30% probability). All hydrogen atoms, noncoordinated triflate anions, and noncoordinated solvent molecules are omitted for clarity. Only the major disordered components of the n-propyl groups are shown.

dx.doi.org/10.1021/ic400096e | Inorg. Chem. 2013, 52, 7394−7410

Table 4. Selected Bond Lengths (Angstroms) and Angles (Degrees) for the Octahedral Geometry of 20

	Bond Lengths		Bond Angles		Bond Angles
Fe1–N11	2.136(3)	N11–Fe1–N12	168.80(13)	N12–Fe1–O12	79.57(11)
Fe1–N12	2.133(3)	N11–Fe1–N31	92.31(13)	N31–Fe1–N32	98.45(13)
Fe1–N31	2.154(3)	N11–Fe1–N32	95.69(12)	N31–Fe1–O11	90.65(12)
Fe1–N32	2.137(3)	N11–Fe1–O11	79.98(12)	N31–Fe1–O12	170.40(12)
Fe1–O11	2.252(3)	N11–Fe1–O12	93.17(11)	N32–Fe1–O11	170.10(12)
Fe1–O12	2.303(3)	N12–Fe1–N31	93.78(13)	N32–Fe1–O12	88.84(12)
		N12–Fe1–N32	92.70(13)	O11–Fe1–O12	82.56(11)
		N12–Fe1–O11	90.55(12)		
$\langle\lambda_{oct}\rangle$	1.012	σ_{oct}^2 (deg^2)	37.09		

residues are shown in Table 5. Steric bulk caused by the ethyl and isopropyl groups make the ester groups noncoordinated to

Table 5. Selected Bond Lengths (Angstroms) and Angles (Degrees) for the Two Tetrahedral Residues in 20

	Bond Lengths		Bond Angles		Bond Angles
			Residue 1		
Fe2–N13	2.022(3)	N13–Fe2–N14	134.35(14)	N14–Fe2–N33	111.27(13)
Fe2–N14	2.025(3)	N13–Fe2–N33	95.59(13)	N14–Fe2–N34	95.89(13)
Fe2–N33	2.048(3)	N13–Fe2–N34	112.84(13)	N33–Fe2–N34	104.38(13)
Fe2–N34	2.057(3)				
$\langle\lambda_{tet}\rangle^a$	1.049	σ_{tet}^2 (deg^2)	207.57		
			Residue 2		
Fe3–N15	2.041(3)	N15–Fe3–N16	104.34(13)	N16–Fe3–N35	110.98(13)
Fe3–N16	2.045(3)	N15–Fe3–N35	95.42(13)	N16–Fe3–N36	95.54(12)
Fe3–N35	2.027(3)	N15–Fe3–N36	112.51(13)	N35–Fe3–N36	135.33(13)
Fe3–N36	2.026(3)				
$\langle\lambda_{tet}\rangle^b$	1.052	σ_{tet}^2 (deg^2)	219.60		

$^a\langle\lambda_{tet}\rangle = \Sigma_{i=1}^{4}(l_i/l_o)^2/4$ $^b\sigma_{tet}^2 = \Sigma_{i=1}^{6}(\theta_i - 109.47°)^2/5$

the metal center in the tetrahedral complex. In the octahedral coordination mode, this bulk results in elongated Fe–O bonds. The tetrahedral N–Fe–N angles vary between 95.4 and 135.3° and are far from the ideal geometry of 109°. The bond lengths in the tetrahedral residues are the shortest among all structures presented in this study. Steric factors seem to play a decisive role in this. Because the enhanced overall steric bulk of the **BEIPrIP^{nPr}** ligand prevents the coordination of the oxygen donors, the nitrogen-donor moieties can approach the iron(II) ion more closely. The remarkable presence of two different coordination geometries of **20** in the solid state explains the presence of the three carbonyl peaks in its IR spectrum (vide infra).

We are not aware of many examples in the literature in which two different coordination geometries of the same molecular metal complex are present within one crystal.[36] Because both geometries of **20** are present in the same unit cell, this indicates that their energies are almost equal and that the transition energy between the two geometries is low. To provide more insight into the ground-state energy difference between both geometries, DFT geometry optimizations were performed at the bp86, SV(P) level. Improved energies were obtained with single-point SCF energy calculations at the b3-lyp TZVP level. In these calculations, simplified versions of the ligands were used in which all alkyl tails were substituted for methyl groups to limit computing time. The resulting calculated structures are in agreement with the octahedral and tetrahedral geometries in the crystal of **20** (Figure 8 and Table 6). Comparison of the calculated structures with the experimental crystal structures shows that the geometry around the iron center is the same and that no clear differences in the overall structures are present. The calculated bond lengths and angles are comparable to the data obtained from the crystal structures of the two different geometries (Tables 4 and 5). The substitution of all alkyls for methyl groups could cause minor differences between the geometry of the crystal structure and the calculated structures, but because all alkyl tails are found on the outside of the overall structures and all of them point away from the metal center, only a small deviation is expected between the energy value of the structure with alkyl chains in comparison to that of the calculated structure with methyl groups. The difference in energy between the two geometries was computed to be 5.6 kcal/mol, favoring the octahedral geometry. This small energy difference points out that the octahedral and tetrahedral structures may well coexist in solution and in the solid state.

The different coordination modes of **BAIP**-type ligands around iron point out that the coordination geometry of this ligand system is quite amendable and sensitive to changes in the overall ligand structure. This could also mean that it may be difficult to point out what the real structure of an active species is during catalysis. It could be possible that multiple species are present in solution and that some of these are kinetically more competent than others. Earlier studies demonstrated the coordination flexibility of **BAIP** ligands.[23] A good example of the coordination flexibility of these ligands is the characterization of $[Fe(\mathbf{BMIP^{nPr}})_2(MeOH)_2](OTf)_2$ in which two MeOH molecules have replaced the ester donors and further rearranged the ligands to coordinate in a mutual cis position. The current study shows that IR spectroscopy provides an insightful view of the coordination mode of the **BAIP** ligands. A combination of solid-state and solution IR spectra indicated the presence of different coordination conformers for complexes **17** and **20** on the basis of the coordinating/noncoordinating nature of the carbonyl moieties. Furthermore, the IR studies indicated that complexes with an imidazole backbone are more prone to rearrangement in solution, involving both dissociation of ester donor moieties and coordination of solvent molecules. The difference in coordination flexibility between the imidazole and benzimidazole ligands can be explained by the more electron-deficient nature of the benzimidazole donor in comparison to that of the imidazole donor and, accordingly, a stronger interaction between the metal and the ester moieties in the benzimidazole complexes.

Magnetic Susceptibility Measurements. The magnetic moments of all reported iron(II) complexes were determined in acetonitrile at 298 K using Evans' NMR method.[37,38] All complexes showed magnetic moments consistent with high-spin (S = 2) iron(II) centers. For complexes **16** and **19**, no magnetic moments were determined, but according to the bond

dx.doi.org/10.1021/ic400096e | Inorg. Chem. 2013, 52, 7394–7410

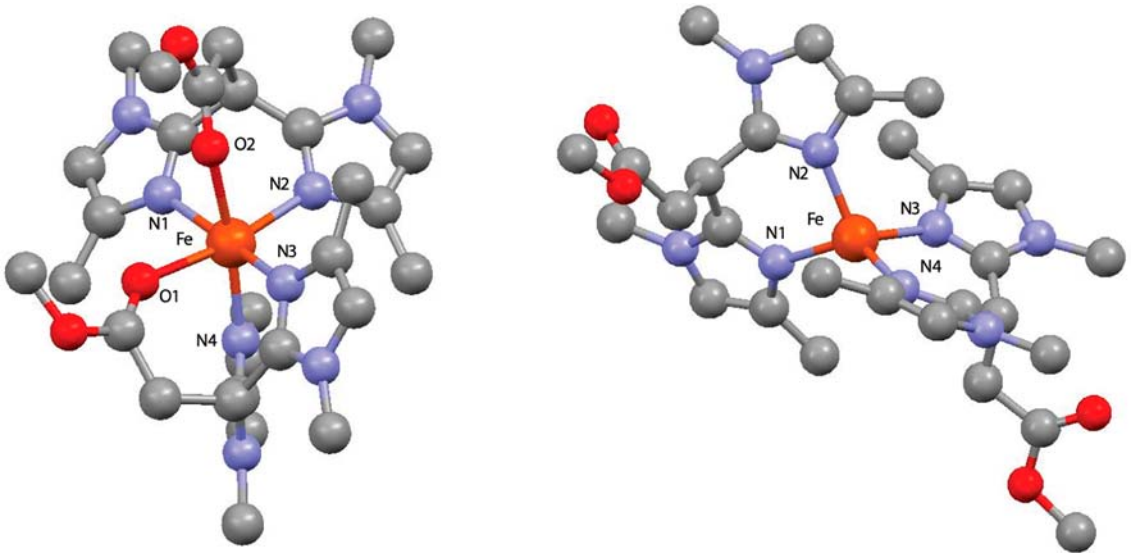

Figure 8. Calculated structures (DFT) of the two geometries of complex **20**.

Table 6. Bond Lengths (Angstroms) and Angles (Degrees) of the Calculated DFT Structures of Complex 20

octahedral				tetrahedral			
Bond Lengths			Bond Angles	Bond Lengths			Bond Angles
Fe−N1	2.186	O1−Fe−N1	88.0	Fe−N1	2.050	N1−Fe−N2	94.9
Fe−N2	2.155	N1−Fe−N2	87.5	Fe−N2	2.051	N2−Fe−N3	111.6
Fe−N3	2.187	N2−Fe−N3	100.4	Fe−N3	2.048	N3−Fe−N4	94.8
Fe−N4	2.154	N3−Fe−O1	83.0	Fe−N4	2.047	N1−Fe−N4	130.4
Fe−O1	2.191	O1−Fe−O2	85.6				
Fe−O2	2.192	O1−Fe−N2	171.8				
		O2−Fe−N4	171.9				

Table 7. Properties of the Synthesized Complexes

complex	C═O position	ν(C═O)(cm^{-1})	$\Delta\nu$(C═O)(cm^{-1})[a]	μ_{EFF} (μ_B)
[Fe(**BMIP^{nPr}**)$_2$](OTf)$_2$ (**14**)	trans	1691	36	5.1
[Fe(**BMIP^{tBu}**)$_2$](OTf)$_2$ (**15**)	trans	1692	33	5.1
[Fe(**BMIP^{AnPr}**)$_2$](OTF)$_2$ (**16**)	trans	n.a.	n.a.	n.a. (HS)[b]
[Fe(**BMBIP^{nPr}**)$_2$](OTf)$_2$ (**17**)	cis, (trans)	1709, 1694	25, 40	5.1
[Fe(**BMBIP^{tBu}**) $_2$](OTf)$_2$ (**18**)	trans	1665	55	5.3
[Fe(**BMBIP^{AnPr}**)$_2$](OTf)$_2$ (**19**)	trans	1628	28	n.a. (HS)[b]
[Fe(**BEiPrIP^{nPr}**)$_2$](OTf)$_2$ (**20**)	cis[c], (trans)	1736[d],1705[c], 1691[c]	2, 29, 43	5.1

[a]Compared to the free ligand. [b]Indicated by Fe−N bond lengths. [c]Octahedral. [d]Tetrahedral.

lengths in the crystal structures of **16** and **19**, a high-spin configuration was also assigned to these complexes. An overview of the spectroscopic properties of complexes **14**−**20** is summarized in Table 7.

CV Measurements. The oxidation potentials of Fe(II) complexes **14**, **18**, and **19** were investigated by means of cyclic voltammetry. These complexes showed (quasi)reversible, single-wave features that indicate clean one-electron Fe(II)/Fe(III) oxidation−reduction processes (Table 8 and Figure 9).

Table 8. Summarized Cyclic Voltammetry Data for Complexes 14, 18, and 19

complex	$E_{1/2}$ (V)	ΔE_p (mV)
[Fe(**BMIP^{nPr}**)$_2$](OTf)$_2$ (**14**)	0.735	175
[Fe(**BMBIP^{tBu}**) $_2$](OTf)$_2$ (**18**)	0.910	80
[Fe(**BMBIP^{AnPr}**)$_2$](OTf)$_2$ (**19**)	0.595	60

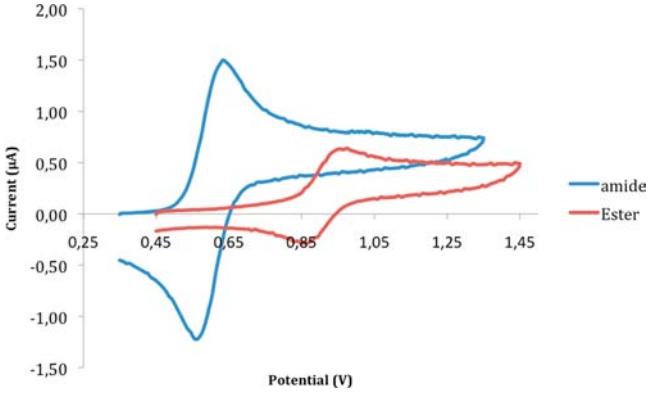

Figure 9. Cyclic voltammograms of complexes **18** and **19**.

The cyclic voltammetry measurements showed that amide complex **19** is oxidized at a much lower potential ($E_{p,a}$ = 0.63

dx.doi.org/10.1021/ic400096e | Inorg. Chem. 2013, 52, 7394−7410

V) in comparison to that of the ester complexes **14** and **18** ($E_{p,a}$ = 0.82 and 0.95 V), making complex **19** more sensitive to oxidation. Complex **19** was at first isolated as an off-white crystalline solid just like the other complexes, but the color of the isolated complex turned red after 1 day of storage. This change in color points to the oxidation of the Fe(II) complex to an Fe(III) complex. The same observation was also made during catalysis where the reaction mixture turned red when **19** was used as the catalyst. The lower oxidation potential of **19** likely results from a combination of (more) electron-deficient benzimidazole donors and strong amide donors (as shown by the short Fe−O distance in the crystal). This combination is also expected to lead to a complex with a diminished coordination flexibility and high conformational integrity. The latter aspect may be reflected in the close-to-Nernstian ΔE_p in CV for the redox change between Fe(II) and Fe(III) in **19**. The observation that complex **14** is oxidized at a lower potential than complex **18** seems to reflect the relative electron-donating abilities of the imidazole donor with respect to the benzimidazole donor groupings.

In Figure 9, the cyclic voltammogram of the benzimidazole amide complex **19** is combined with the voltammogram of the benzimidazole ester complex **18**. Unfortunately, no CV measurements could be carried out on amide complex **16** because of to the low yield of the complex.

Oxidation Catalysis. The ability of complexes **14**−**20** to catalyze the oxidation of olefins was investigated by using cyclooctene as a benchmark substrate (Scheme 4). The

Scheme 4. General Representation of the Oxidation of Cyclooctene

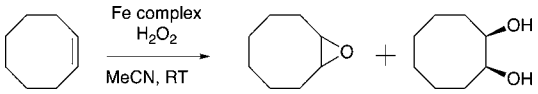

oxidations were carried out in acetonitrile at ambient temperature and under a nitrogen atmosphere, using H_2O_2 as the sacrificial oxidant. The oxidant was added dropwise over a period of 20 min to minimize the chance for peroxide disproportionation. The reactions were carried out with different ratios among the catalyst, oxidant, and substrate. In all cases, the substrate was present in a large excess (oxidant limiting conditions). The reactions were monitored by GC, and samples were taken 1 and 3 h after the first drop of oxidant was added to the reaction mixture as well as after running the reaction for 1 night (Table 9).

Overall, all tested complexes are able to oxidize cyclooctene, albeit with rather low TONs and low productive H_2O_2 consumption. This observation is in line with earlier studies on the oxidation of cyclooctene with $[Fe(\mathbf{BMIP^{nPr}})_2](OTf)_2$ and $[Fe(\mathbf{BMIP^{nPr}})_2](BPh_4)_2$.[23] In the present case, productive H_2O_2 conversion varies between 5 and 25% after 1 night of reaction time, which corresponds to a range of 0−10 turnovers per iron. For the first group of complexes (**14**−**16**), complex **14** was the most active. The use of 20 equiv of H_2O_2 per iron resulted in a productive conversion of H_2O_2 from 23 to 25% after 1 night with different amounts of substrate (500 and 1000 equiv, respectively). These conditions resulted in epoxide to diol ratios of 1.5:1 and 1.6:1. An increase in the oxidant loading to 100 equiv resulted in an increase in the turnover number to 10 (10% productive H_2O_2 consumption) and a change in the epoxide/cis-diol ratio to 5.5:1. For complexes **15** and **16**, the overall catalytic characteristics are lower, and only minor traces of diol are formed. The overall catalytic activity of **14** is the highest among the complexes tested here.

The reactivity of the group of benzimidazole complexes (**17**−**19**) is comparable to the activity of complex **16**. The most interesting result from this group of complexes was obtained with amide complex **19**. In this case, equal amounts of epoxide and cis-diol were formed at a catalyst/oxidant/substrate ratio of 1:20:1000. Although the amount of cis-diol product is lower than the amount produced by complex **14**, a larger amount of epoxide was formed in the latter case. During the catalytic reactions with complex **19**, a change in color from off-white to red was observed upon the addition of the oxidant (vide supra). For all of the other complexes, the color of the solution changed to dark-yellow/orange after the addition of hydrogen peroxide. Because of its crystal structure, complex **17** $[Fe(\mathbf{BMBIP^{nPr}})_2](OTf)_2$ was expected to be a good candidate for a cis-dihydroxylation catalyst as a result of the cis coordination of the two carbonyl groups. However, **17** gave a 3:1 ratio of epoxide/cis-diol product at best. This observation adds to the notion that the cisoid structure, as observed by X-ray crystallography, is one of several conformers of **17** and apparently does not stand out in its kinetic competence during catalysis. Complex **20** was among the least active complexes in this study. A small amount of epoxide was formed, and, in some cases, a small trace of diol was observed with an H_2O_2 conversion of between 3 and 7%.

Few other Fe-based catalysts, in particular, those based on a mixed N,N,O ligand manifold, are known to perform cis-dihydroxylations of alkenes using H_2O_2, and cyclooctene is not always included as a substrate in these studies. The Ph-DPAH-based system reported by Que et al. shows a selectivity toward the diol in the oxidation of cyclooctene of 14:1 with a TON value of 7.0 toward the diol product.[16] Later, this system was optimized through ligand derivatization to yield exclusively the diol product in styrene oxidation (TON = 9.4) and 1-octene oxidation (TON = 7.7).[39] Cyclooctene was not included as a substrate in this study. The same group also reported on a polydentate mixed N,O ligand derived from Kemp's acid in which the corresponding Fe(II) complex is able to oxidize 1-octene to the epoxide/diol in a 1:6 ratio, albeit with a TON value of lower than 1 per iron.[40] These data show that turnover values in cis-dihydroxylation reactions using mixed N,O ligands in combination with iron are, in general, low. The cis-dihydroxylation activity of nonheme iron complexes derived from all-nitrogen ligands has been described somewhat more extensively (vide supra). The most active systems reported so far are derived from the PyTACN ligand system reported by the group of Costas. These systems show TON values for diols of up to 140 and diol/epoxide ratios of up to 4.9 in the oxidation of cyclooctene (300 equiv of H_2O_2 was used). All of these studies used large excesses (∼1000 equiv) of alkene substrate per iron.[41]

The overall low activity of the complexes presented here poses a challenge for their further improvement or even practical use. Issues that could be at play here, in addition to metal release from the ligand manifold, are the structural integrity of the complexes and diol product inhibition. Our investigation of the structure of iron complexes based on the **BAIP**-ligand family has shown the coordination flexibility of these ligands in solution as well as in the solid state. Accordingly, this may lead to multiple species under catalytic conditions, with a variation in activity and specificity. For the

dx.doi.org/10.1021/ic400096e | Inorg. Chem. 2013, 52, 7394−7410

Table 9. Overview of the Catalytic Results

			epoxide[a]			cis-diol[a]				
complex	eq. H_2O_2	eq. substrate	1 h	3 h	1 night	1 h	3 h	1 night	conversion (%)[b]	epoxide/diol ratio[c]
14	20	500	3.3	3.0	2.7	1.4	1.2	1.8	23	1.5:1
	20	1000	3.7	3.1	3.1	1.5	1.3	1.9	25	1.6:1
	100	1000	7.1	6.6	8.2	1.0	1.0	1.5	10	5.5:1
15	20	500	2.8	2.7	2.4				12	> 100:1
	20	1000	3.4	3.1	2.4				12	> 100:1
	100	1000	5.1	5.3	5.7				6	> 100:1
16	20	500	1.0	1.1	0.9				5	> 100:1
	20	1000	1.3	1.5	1.0	0.1	0.1	0.1	5	10:1
	100	1000	2.5	3.4	4.8			0.1	5	48:1
17	20	500	1.6	1.8	1.7	0.1	0.2	0.4	11	4.3:1
	20	1000	1.7	1.6	1.5	0.3	0.3	0.5	10	3:1
	100	1000	3.4	4.0	6.0	0.1	0.1	0.1	6	60:1
18	20	500	1.1	1.0	0.8				4	> 100:1
	20	1000	1.4	1.1	0.9		0.1		5	> 100:1
	100	1000	2.3	2.8	3.3				3	> 100:1
19	20	500	1.0	1.1	0.7	0.8	0.7	0.5	6	1.4:1
	20	1000	1.2	1.3	0.8	1.4	1.3	0.8	8	1:1
	100	1000	2.9	3.3	4.3	0.4	0.6	0.1	4	43:1
20	20	500	1.0	1.0	1.2	0.1	0.1	0.1	7	12:1
	20	1000	1.3	1.3	1.6	0.1	0.1	0.1	9	16:1
	100	1000	2.0	2.3	2.9			0.1	3	29:1

[a]Yields expressed as turnover numbers (TON = mol product/mol catalyst). [b]Conversion of H_2O_2 into epoxide and cis-diol after 1 night. [c]After 1 night.

BAIP ligands, our investigations show that a change from imidazole to benzimidazole donors prevents ester dissociation from the metal. On the one hand, this reduces the number of solution species, but on the other hand the creation of vacant sites on the metal is hampered. In effect, this has led to a lower activity for the benzimidazole complexes. Another factor that influences product formation and turnover, which is less discussed, is the possibility of product inhibition. Although reaction mixtures involving H_2O_2 tend to be acidic, the formation of stable iron-diolate complexes cannot be excluded. Such complexes seem to lack sufficient open coordination sites to accommodate a cis-dihydroxylation pathway and are proposed to be inactive. We have previously reported on Fe-catecholate complexes derived from **BAIP** ligands and found that these are rather stable or show catechol-based chemistry.[22] The release of diols from Fe-diolate complexes, leading to increased TONs, may be accomplished by the use of a proper reaction medium. This matter is currently under investigation in our laboratories

CONCLUSIONS

We have presented an extension of the **BAIP** ester ligand family and have studied the coordination chemistry of the new ligands toward $Fe(OTf)_2$. These studies have shown the intrinsic property of these ligands to bind to iron in a facial N,N,O manner, thereby mimicking the 2-His-1-carboxylate facial triad found in mononuclear nonheme iron enzymes. The coordination flexibility of the ligands also manifested itself in these studies, where in addition to trans bis-ligand arrangements, cis arrangements are also possible and where tetrahedral, all-nitrogen coordination can be enforced by the steric bulk. Although these studies have not led to the development of an improved olefin cis-dihydroxylation catalyst, they do provide design tools for the further development of biomimetic mononuclear nonheme iron complexes and for steering the reactivity of such complexes in catalysis. In particular, the role of benzimidazole donors in providing a well-defined tripodal coordination mode for the ligands in solution, the electron-rich nature of amide donors that may help to stabilize the higher oxidation states of the metal, and the subtle role of steric factors in the balance between site isolation and coordination-mode integrity are of interest. These considerations are currently included in the design of new ligands and their corresponding nonheme iron complexes, with the aim of arriving at site-isolated mononuclear complexes "capped" by a single N,N,O ligand that feature enhanced activities in the catalytic cis-dihydroxylation of olefins.

EXPERIMENTAL SECTION

General. Air-sensitive reactions were carried out under an inert N_2 atmosphere using standard Schlenk techniques. The solvents were dried and distilled before use. The chemicals were commercially obtained and used as received or were reproduced from the literature. ^1H and ^{13}C NMR spectra were recorded with a Varian 400 spectrometer at 400 and 100 MHz, respectively, operating at 25 °C. Infrared spectra were recorded with a Perkin-Elmer Spectrum One FTIR instrument. Solution IR measurements were recorded with a Mettler Toledo ReactIR 1000 spectrometer with a SiComp probe placed in a Schlenk tube under a N_2 atmosphere. GC-MS measurements were recorded with a Perkin-Elmer Autosystem XL gas chromatograph with an attached Perkin-Elmer Turbomass Upgrade mass spectrometer. High-resolution ESI-MS data were acquired with a Waters LCT Premier XE machine. Solution magnetic moments were determined by the Evans NMR method in acetone-d_6/cyclohexane (95/5 v/v) or in acetonitrile-d_3/cyclohexane (95/5 v/v) at 25 °C.[37,38] GC analyses were performed with a Perkin-Elmer Clarus 500 GC (30 m, Econo-Cap EC-5) with an FID detector. Elemental microanalyses were carried out by the Mikroanalytisches Laboratorium KOLBE, Mülheim an der Ruhr, Germany. Cyclic voltammograms were recorded in a single-compartment cell under a dry N_2 atmosphere. The cell was equipped with a Pt working electrode, a Pt wire counter electrode, and a Ag/AgCl reference electrode.

dx.doi.org/10.1021/ic400096e | Inorg. Chem. 2013, 52, 7394−7410

Potential control was achieved with a PAR model 263A potentiostat. Bis(1-methylimidazol-2-yl)methane (**1**),[26,27] bis(1-methylbenzimidazol-2-yl)methane (**2**),[28] propyl 3,3-bis(1-methyl(benz)imidazol-2-yl)-propionate (**BMIP^{nPr}** (**3**), **BMBIP^{nPr}** (**4**)),[25] 3,3-bis(1-methyl(benz)-imidazol-2-yl)propionic acid (**7**,**10**),[25] propyl 3,3-bis(1-ethyl-4-isopropylimidazol-2-yl)propionate (**BEiPrIP^{nPr}**, (**13**)),[30] $Fe(OTf)_2{\cdot}2MeCN$,[31] and [Fe(**BMIP^{nPr}**)$_2$](OTf)$_2$ (**14**)[23] were prepared according to published procedures.

*tert-Butyl 3,3-Bis(1-methylimidazol-2-yl)propionate, **BMIP^{tBu}** (**5**).* A solution of *n*-butyllithium (0.48 mL, 0.77 mmol, 1.6 M in hexanes) was added dropwise to a stirring solution of bis(1-methylimidazol-2-yl)methane (**1**) (134 mg, 761 μmol) in THF (4 mL) at −78 °C. The greenish solution was stirred for 1 h at −78 °C, followed by the dropwise addition of *tert*-butyl bromoacetate (115 μL, 779 μmol). The temperature of the mixture was allowed to rise to room temperature, and the mixture was quenched with H_2O (10 mL). All volatiles were evaporated in vacuo, the water layer was extracted with ethyl acetate (4 × 10 mL), and the combined organic layers were dried over magnesium sulfate, filtered, and concentrated in vacuo. The product was obtained as a clear yellow oil (216 mg, 90%). ^{1}H NMR (400 MHz, $CDCl_3$, 25 °C): δ = 1.16 (s, 9H, OC(CH_3)$_3$), 3.03 (d, 2H, $^3J_{HH}$ = 7.6 Hz, CHCH_2), 3.32 (s, 6H, NCH_3), 4.74 (t, 1H, $^3J_{HH}$ = 8.0 Hz, CHCH$_2$), 6.58 (d, 2H, $^3J_{HH}$ = 0.8 Hz, H_{imid}), 6.71 (d, 2H, $^3J_{HH}$ = 0.8 Hz, H_{imid}). ^{13}C {1H} NMR (100 MHz, $CDCl_3$, 25 °C): δ = 28.0, 32.9, 34.7, 37.6, 80.9, 122.1, 127.0, 145.4, 170.3. IR (solid) ν (cm^{-1}): 3107.0, 2977.4, 2932.3, 1725.5, 1520.5, 1491.0, 1455.9, 1411.4, 1392.9, 1366.0, 1310.9, 1280.4, 1249.7, 1151.1, 1133.7, 857.6, 763.7, 738.3. ESI-MS: m/z = 291.182 ([M + H]$^+$, calcd 291.182).

*tert-Butyl 3,3-Bis(1-methylbenzimidazol-2-yl)propionate, **BMBIP^{tBu}** (**6**).* A solution of *n*-butyllithium (0.75 mL, 1.2 mmol, 1.6 M in hexanes) was added dropwise to a stirring solution of **2** (308 mg, 1.11 mmol) in THF (20 mL) at −78 °C. The greenish solution was stirred for 1 h at −78 °C, followed by the dropwise addition of *tert*-butyl bromoacetate (165 μL, 1.11 mmol). The temperature of the mixture was allowed to rise to room temperature, and the mixture was quenched with H_2O (15 mL). All volatiles were evaporated in vacuo, the water layer was extracted with ethyl acetate (2 × 25 mL), and the combined organic layers were dried over magnesium sulfate, filtered, and concentrated in vacuo. The product was obtained as an off-white solid (407 mg, 94%). ^{1}H NMR (400 MHz, $CDCl_3$, 25 °C): δ = 1.33 (s, 9H, OC(CH_3)$_3$), 3.50 (d, 2H, $^3J_{HH}$ = 7.6 Hz, CHCH_2), 3.81 (s, 6H, NCH_3), 5.48 (m, 1H, CHCH$_2$), 7.27 (m, 6H, $H_{benzimid}$), 7.76 (m, 2H, $H_{benzimid}$). ^{13}C {1H} NMR (100 MHz, $CDCl_3$, 25 °C): δ = 28.2, 30.7, 36.1, 37.4, 81.7, 109.6, 119.7, 122.7, 123.3, 136.5, 151.2, 169.8. IR (solid) ν (cm^{-1}): 3046.3, 2934.1, 2871.2, 1719.6, 1614.6, 1467.3, 1438.8, 1359.7, 1331.5, 1145.2, 981.2, 741.9. ESI-MS: m/z = 391.215 ([M + H]$^+$, calcd 391.213).

*NHS 3,3-Bis(1-methylimidazol-2-yl)propionate (**8**).* N-Hydroxysuccinimide (373 mg, 3.25 mmol) and *N*,*N*′-dicyclohexylcarbodiimide (670 mg, 3.25 mmol) were added to a stirring suspension of **7** (759 mg, 3.24 mmol) in dry THF (250 mL), followed by the addition of pyridine (1.5 mL, 18.5 mmol). A reflux condenser was put on top of the flask, and the reaction mixture was stirred in an oil bath at 40 °C overnight after which time the reaction mixture was still a white suspension. After the reaction mixture was stirred at 45 °C for an additional 3 h, the white solid particles were filtered off and the evaporation of the solvent in vacuo yielded a yellow/white solid that was dissolved in dichloromethane. The precipitated urea was filtered off, and the dichloromethane was evaporated in vacuo. The remaining solid was dissolved again in dichloromethane, and the precipitate was filtered off. This cycle was repeated until no further precipitate was formed (three cycles). The yellowish solid was recrystallized from a dichloromethane/diethyl ether mixture at −30 °C overnight, yielding an off-white solid (450 mg, 43%). This preparation was not entirely pure, as some dicyclohexylurea was present according to NMR. ^{1}H NMR (400 MHz, $CDCl_3$, 25 °C): δ = 2.63 (s, 4H, C(O)CH_2), 3.25 (d, 2H, $^3J_{HH}$ = 6.4 Hz, CHCH_2), 3.48 (s, 6H, NCH_3), 4.98 (t, 1H, $^3J_{HH}$ = 8.0 Hz, CHCH$_2$), 6.72 (s, 2H, H_{im}), 6.87 (s, 2H, H_{im}). ^{13}C {1H} NMR (100 MHz, DMSO-d_6, 25 °C): δ = 25.7, 32.3, 33.1, 38.8, 123.1, 125.9, 145.8, 173.2, 174.1. ESI-MS: m/z = 332.135 ([M + H]$^+$, calcd 332.136).

*3,3-Bis(1-methylimidazol-2-yl)-N-propylpropanamide, **BMIP^{AnPr}** (**9**).* Propylamine (112 μL, 1.38 mmol) was added to a solution of **8** (450 mg, 1.36 mmol) in dichloromethane (20 mL). The colorless solution was stirred for 48 h at room temperature. The reaction mixture was washed with a saturated $NaHCO_3$ solution (2 × 15 mL) and H_2O (2 × 15 mL). The combined aqueous layers were extracted with dichloromethane (1 × 15 mL), and the combined organic layers were dried over magnesium sulfate, filtered, and evaporated in vacuo, yielding a white solid that was recrystallized from a dichloromethane/diethyl ether mixture (95 mg, 25%). ^{1}H NMR (400 MHz, $CDCl_3$, 25 °C): δ = 0.81 (t, 3H, $^3J_{HH}$ = 7.4 Hz, NHCH$_2$CH$_2$CH_3), 1.40 (sextet, 2H, $^3J_{HH}$ = 7.2 Hz, NHCH$_2$CH_2CH$_3$), 3.11 (m, 2H, NHCH_2CH$_2$CH$_3$), 3.14 (d, 2H, $^3J_{HH}$ = 7.6 Hz, CHCH_2), 3.50, (s, 6H, NCH_3), 4.83 (t, 1H, $^3J_{HH}$ = 7.2 Hz, CHCH$_2$), 6.53 (m, 1H, NHCH$_2$CH$_2$CH$_3$), 6.77 (s, 2H, H_{im}), 6.93 (s, 2H, H_{im}). ^{13}C {1H} NMR (100 MHz, $CDCl_3$, 25 °C): δ = 11.5, 22.8, 33.3, 33.8, 39.1, 41.5, 122.1, 126.8, 145.8, 170.4. IR (solid) ν (cm^{-1}): 3231.9, 3050.7, 2970.1, 2937.1, 2875.7, 1650.6, 1562.8, 1489.0, 1473.9, 1278.7, 1237.9, 1133.3, 1084.1, 971.1, 924.7, 843.0, 761.0, 738.2, 694.3. ESI-MS: m/z = 276.187 ([M + H]$^+$, calcd 276.182).

*NHS 3,3-Bis(1-methylbenzimidazol-2-yl)propionate (**11**).* N-Hydroxysuccinimide (166 mg, 1.44 mmol) and *N*,*N*′-dicyclohexylcarbodiimide (303 mg, 1.47 mmol) were added to a stirring suspension of **10** (480 mg, 1.44 mmol) in dry THF (200 mL), followed by the addition of pyridine (1.5 mL, 18.5 mmol). A reflux condenser was put on top of the flask, and the reaction mixture was stirred in an oil bath at 35 °C for 3 h, followed by stirring at room temperature overnight. The reaction mixture became a clear yellow solution upon heating to 35 °C again, and stirring at 35 °C was continued for another 8 h, followed by stirring at room temperature for 3 days. Some white precipitate (*N*,*N*′-dicyclohexylurea) was present that was filtered off, followed by the evaporation of the solvent in vacuo, yielding a yellow-white solid that was dissolved in dichloromethane. The precipitated urea was filtered off, and the dichloromethane was evaporated in vacuo. The remaining solid was dissolved again in dichloromethane, and the precipitate was filtered off. This cycle was repeated until no more precipitate was formed (four cycles). The yellowish solid was recrystallized from a dichloromethane/diethyl ether mixture at −30 °C overnight, yielding a slightly yellow solid (529 mg, 85%). ^{1}H NMR (400 MHz, $CDCl_3$, 25 °C): δ = 2.76 (s, 4H, C(O)CH_2), 3.73 (s, 6H, NCH_3), 3.94 (d, 2H, $^3J_{HH}$ = 7.6 Hz, CHCH_2), 5.50 (t, 1H, $^3J_{HH}$ = 7.6 Hz, CHCH$_2$), 7.27 (m, 6H, $H_{benzimid}$), 7.79 (m, 2H, $H_{benzimid}$). ^{13}C {1H} NMR (100 MHz, $CDCl_3$, 25 °C): δ = 25.7, 30.5, 33.5, 35.8, 109.6, 120.2, 122.7, 123.4, 136.6, 142.0, 150.1, 166.8, 168.8. IR (solid) ν (cm^{-1}): 2936.7, 1813.9, 1782.0, 1728.3, 1502.5, 1469.4, 1438.2, 1363.4, 1287.3, 1197.2, 1156.2, 1094.8, 1062.6, 980.3, 869.0, 809.2, 743.4. ESI-MS: m/z = 432.163 ([M + H]$^+$, calcd 432.167).

*3,3-Bis(1-methylbenzimidazol-2-yl)-N-propylpropanamide, **BMBIP^{AnPr}** (**12**).* Propylamine (48 μL, 580 μmol) was added to a solution of **11** (250 mg, 579 μmol) in dichloromethane (10 mL). The colorless solution was stirred overnight at room temperature. The reaction mixture was washed with a saturated $NaHCO_3$ solution (2 × 5 mL) and H_2O (1 × 5 mL). The combined aqueous layers were extracted with dichloromethane (1 × 5 mL), and the combined organic layers were dried over magnesium sulfate, filtered, and evaporated in vacuo, yielding a white solid (195 mg, 90%). ^{1}H NMR (400 MHz, $CDCl_3$, 25 °C): δ = 0.77 (t, 3H, $^3J_{HH}$ = 7.4 Hz, NHCH$_2$CH$_2$CH_3), 1.37 (sextet, 2H, $^3J_{HH}$ = 7.2 Hz, NHCH$_2$CH_2CH$_3$), 3.12 (q, 2H, $^3J_{HH}$ = 6.7 Hz, NHCH_2CH$_2$CH$_3$), 3.40 (d, 2H, $^3J_{HH}$ = 6.8 Hz, CHCH_2), 3.73 (s, 6H, NCH_3), 5.32 (t, 1H, $^3J_{HH}$ = 7.2 Hz, CHCH$_2$), 6.38 (m, 1H, NHCH$_2$CH$_2$CH$_3$), 7.29 (m, 6H, $H_{benzimid}$), 7.73 (m, 2H, $H_{benzimid}$). ^{13}C {1H} NMR (100 MHz, $CDCl_3$, 25 °C): δ = 11.4, 22.8, 30.3, 31.1, 35.4, 39.3, 41.6, 109.5, 120.0, 122.4, 123.0, 136.4, 142.3, 152.1, 170.3. IR (solid) ν (cm^{-1}): 3235.1, 3057.2, 2930.0, 1656.2, 1555.9, 1507.8, 1464.0, 1439.9, 1395.5, 1281.9, 1262.4, 1240.0, 1092.7, 773.6, 740.3. Anal. Calcd for $C_{22}H_{25}N_5O$ (375.47): C 70.38, H 6.71, N 18.65; found C 70.59, H 7.05, N 18.43.

dx.doi.org/10.1021/ic400096e | *Inorg. Chem.* 2013, 52, 7394−7410

Table 10. Experimental Details of the Crystal Structures for 14−16

	14	15	16
formula	$[C_{28}H_{40}FeN_8O_4](CF_3O_3S)_2 \cdot 1.95(CH_3CN)$	$[C_{30}H_{44}FeN_8O_4](CF_3O_3S)_2$ + disordered acetonitrile	$[C_{28}H_{42}FeN_{10}O_2](CF_3O_3S)_2$
fw	986.73	934.72[a]	904.71
cryst color	colorless	colorless	colorless
cryst size (mm^3)	0.63 × 0.42 × 0.04	0.18 × 0.16 × 0.12	0.90 × 0.21 × 0.03
cryst syst	triclinic	monoclinic	triclinic
space group	$P\bar{1}$ (No. 2)	$P2_1/n$ (No. 14)	$P\bar{1}$ (No. 2)
a (Å)	14.3823(2)	17.2165(5)	8.6294(5)
b (Å)	14.6648(4)	13.1126(4)	10.7097(8)
c (Å)	22.2031(7)	20.2556(13)	11.4184(6)
α (deg)	87.999(1)	90	65.829(4)
β (deg)	88.800(1)	91.338(2)	88.557(3)
γ (deg)	89.251(1)	90	81.683(2)
V ($Å^3$)	4678.7(2)	4571.4(4)	951.95(10)
Z	4	4	1
D_{calc} (g/cm^3)	1.401	1.358[a]	1.578
$(\sin\theta/\lambda)_{max}$ ($Å^{-1}$)	0.55	0.53	0.48
reflns. measured/unique	47 185/12 969	46 455/5600	6170/1681
parameters/restraints	1227/469	545/195	334/187
R1/wR2 [$I > 2\sigma(I)$]	0.0680/0.1657	0.0488/0.1275	0.0665/0.1626
R1/wR2 (all reflns.)	0.1102/0.1909	0.0628/0.1355	0.0827/0.1741
S	1.078	1.148	1.106
ρ(min/max) ($eÅ^{-3}$)	−0.61/1.37	−0.85/0.68	−0.50/0.70

[a]Derived values do not contain the contribution of the disordered solvent.

*[Fe(**BMIP^{tBu}**)$_2$](OTf)$_2$ (**15**).* To a solution of **BMIP^{tBu}** (**5**) (216 mg, 744 μmol) in acetonitrile (2 mL) was added a solution of $Fe(OTf)_2 \cdot 2MeCN$ (171 mg, 370 μmol) in acetonitrile (2 mL), and the yellowish reaction mixture was stirred for 1 h at room temperature. The solvent was evaporated in vacuo, and the remaining brown solid was recrystallized from an acetonitrile/diethyl ether mixture at −30 °C overnight to optimize the yield. The product was obtained as a brown crystalline solid (270 mg, 95%). Single crystals suitable for X-ray diffraction were obtained by the slow vapor diffusion of diethyl ether into a solution of **15** in acetonitrile. IR (solid) ν (cm^{-1}): 2983.2, 1692.2, 1506.7, 1396.5, 1370.3, 1258.1, 1223.5, 1144.1, 1029.4, 988.7, 962.1, 948.2, 852.7, 831.8, 754.3, 734.4. Solution magnetic moment (Evans' method): $\mu_{eff} = 5.1\mu_B$. ESI-MS: m/z = 785.235 ([M-OTf]$^+$, calcd 785.236).

*[Fe(**BMIP^{AnPr}**)$_2$](OTf)$_2$ (**16**).* Compound **9** (13 mg, 48 μmol) was mixed with $Fe(OTf)_2 \cdot 2MeCN$ (11 mg, 24 μmol) in acetonitrile (16 mL) prior to using it in catalysis. Single crystals were grown from the remaining solution by the slow vapor diffusion of diethyl ether into it for X-ray analysis, and no further analysis was performed on the crystals.

*[Fe(**BMBIP^{nPr}**)$_2$](OTf)$_2$ (**17**).* To a solution of **BMBIP^{nPr}** (**4**) (195 mg, 518 μmol) in methanol (5 mL) was added a solution of $Fe(OTf)_2 \cdot 2MeCN$ (114 mg, 259 μmol) in methanol (4 mL), and the reaction mixture was stirred for 40 min at room temperature. The solvent was evaporated in vacuo, and the remaining white solid was recrystallized from an acetonitrile/diethyl ether mixture at −30 °C overnight to optimize the yield. The solvent, which had a deep-red color, was removed with a cannula, and the remaining crystalline solid was washed with diethyl ether and dried in vacuo. The product was obtained as an off-white crystalline solid (254 mg, 89%). Single crystals suitable for X-ray diffraction were obtained by the slow vapor diffusion of diethyl ether into a solution of **17** in acetonitrile. IR (solid) ν (cm^{-1}): 3510.2, 3058.2, 2967.6, 1708.8, 1693.7, 1618.4, 1493.7, 1455.6, 1401.0, 1258.5, 1208.1, 1160.5, 1030.6, 927.1, 739.1. Solution magnetic moment (Evans' method): $\mu_{eff} = 5.1\mu_B$. Anal. Calcd for $C_{46}H_{48}F_6FeN_8O_{10}S_2$ (1106.89): C 49.91, H 4.37, N 10.12; found C 49.39, H 4.53, 10.03.

*[Fe(**BMBIP^{tBu}**)$_2$](OTf)$_2$ (**18**).* To a solution of **BMBIP^{tBu}** (**6**) (158 mg, 405 μmol) in methanol (5 mL) was added a solution of $Fe(OTf)_2 \cdot 2MeCN$ (89 mg, 203 μmol) in methanol (5 mL), and the yellowish reaction mixture was stirred for 45 min at room temperature. The solvent was evaporated in vacuo, and the remaining off-white solid was recrystallized from an acetonitrile/diethyl ether mixture at −30 °C overnight to optimize the yield. The solvent, which had a brownish color, was removed with a cannula, leaving the white crystalline solid (198 mg, 86%). Single crystals suitable for X-ray diffraction were obtained by the slow vapor diffusion of diethyl ether into a solution of **18** in acetonitrile. IR (solid) ν (cm^{-1}): 2981.9, 1665.1, 1490.5, 1454.0, 1418.2, 1398.0, 1373.2, 1260.1, 1226.1, 1149.8, 1029.5, 1010.5, 995.1, 844.5, 745.9. Solution magnetic moment (Evans' method): $\mu_{eff} = 5.3\mu_B$. ESI-MS: m/z = 985.294 ([M − OTf]$^+$, calcd 985.298).

*[Fe(**BMBIP^{AnPr}**)$_2$](OTf)$_2$ (**19**).* To a solution of **BMBIP^{AnPr}** (**12**) (154 mg, 410 μmol) in methanol (7 mL) was added a solution of $Fe(OTf)_2 \cdot 2MeCN$ (90 mg, 205 μmol) in methanol (4 mL), and the reaction mixture was stirred for 30 min at room temperature. The solvent was evaporated in vacuo, and the remaining off-white solid was recrystallized from an acetonitrile/diethyl ether mixture at −30 °C overnight to optimize the yield. The solvent was removed with a cannula, leaving the off-white crystalline solid (178 mg, 79%). Single crystals suitable for X-ray diffraction were obtained by the slow vapor diffusion of diethyl ether into a solution of **19** in acetonitrile. The off-white crystalline solid turned red after 1 day (in a Schlenk tube under an N_2 atmosphere). IR (solid) ν (cm^{-1}): 3297.7, 3104.9, 2965.1, 1628.3, 1565.0, 1504.9, 1481.0, 1454.8, 1277.0, 1244.4, 1223.3, 1151.7, 1028.1, 741.0. ESI-MS: m/z = 955.292 ([M − OTf]$^+$, calcd 955.299).

*[Fe(**BEiPrIP^{nPr}**)$_2$](OTf)$_2$ (**20**).* $Fe(OTf)_2 \cdot 2MeCN$ (86 mg, 197 μmol) was added to a stirring solution of **BEiPrIP^{nPr}** (**13**) (153 mg, 394 μmol) in methanol (4 mL), and the dark-brown solution was stirred for 30 min at room temperature. The solvent was evaporated in vacuo, and the remaining dark oil was recrystallized twice from an acetonitrile/diethyl ether mixture at −30 °C, leaving a yellow crystalline solid that was washed with diethyl ether (50 mg, 34%). Crystals suitable for X-ray diffraction were obtained by the slow vapor diffusion of diethyl ether into a solution of **20** in acetonitrile. IR (solid) ν (cm^{-1}): 3109.1, 2968.3, 2879.0, 1736.0, 1704.8, 1691.5, 1583.1, 1497.1, 1495.2, 1388.1, 1365.3, 1258.6, 1223.6, 1147.5, 1087.4, 1030.6, 975.4, 803.0. Solution magnetic moment (Evans' method): $\mu_{eff} = 5.1\mu_B$. ESI-MS: m/z = 981.455 ([M − OTf]$^+$, calcd 981.454).

Catalysis Protocol. To a solution of catalyst (3 μmol) in acetonitrile (2 mL) was added *cis*-cyclooctene (500 or 1000 equiv) and

dx.doi.org/10.1021/ic400096e | Inorg. Chem. 2013, 52, 7394−7410

Table 11. Experimental Details of the Crystal Structures for 17−19

	17	18	19
formula	$[C_{44}H_{48}FeN_8O_4](CF_3O_3S)_2{\cdot}2(CH_3CN)$	$[C_{46}H_{52}FeN_8O_4](CF_3O_3S)_2{\cdot}5(CH_3CN)$	$[C_{44}H_{50}FeN_{10}O_2](CF_3O_3S)_2{\cdot}2(CH_3CN)$
fw	1189.00	1340.22	1187.04
cryst color	colorless	colorless	yellow
cryst size (mm^3)	0.36 × 0.09 × 0.09	0.42 × 0.10 × 0.08	0.57 × 0.30 × 0.12
cryst syst	orthorhombic	monoclinic	monoclinic
space group	*Pnna* (No. 52)	$P2_1/c$ (No. 14)	$P2_1/c$ (No. 14)
a (Å)	16.6451(2)	11.7689(2)	14.9769(1)
b (Å)	18.8376(3)	26.0832(6)	11.8607(1)
c (Å)	17.5683(3)	22.7901(6)	17.6525(2)
α (deg)	90	90	90
β (deg)	90	112.8675(8)	122.6929(5)
γ (deg)	90	90	90
V ($Å^3$)	5508.61(14)	6446.1(3)	2638.96(4)
Z	4	4	2
D_{calc} (g/cm^3)	1.434	1.381	1.494
$(\sin\theta/\lambda)_{max}$ ($Å^{-1}$)	0.55	0.56	0.65
reflns. measured/unique	44 453/3850	52 160/9198	45 526/6063
parameters/restraints	388/81	858/267	366/0
R1/wR2 [$I > 2\sigma(I)$]	0.0597/0.1721	0.0632/0.1562	0.0418/0.1173
R1/wR2 (all reflns.)	0.0833/0.1897	0.1127/0.1851	0.0552/0.1275
S	1.057	1.077	1.093
ρ(min/max) ($eÅ^{-3}$)	−0.34/1.30	−0.38/0.53	−0.60/0.64

acetonitrile (to bring the total volume to 2.5 mL). 1,2-Dibromobenzene (10 μL) was added as internal standard, and subsequently 0.5 mL of oxidant solution (20 or 100 equiv, diluted from 35% aqueous H_2O_2 with acetonitrile) was added dropwise over 20 min. The reaction mixture was stirred at room temperature, and after 1 h the first sample was taken. Diethyl ether was added to the sample to precipitate the iron complex, after which it was analyzed by GC.

X-ray Crystal Structure Determinations. Reflections were recorded with a Nonius KappaCCD diffractometer with a rotating anode and a graphite monochromator (λ = 0.71073 Å) at a temperature of 150(2) K. Intensity data were integrated with Eval14[42] (compounds **14** and **16**), Eval15[43] (compound **15**), or HKL2000[44] (compounds **17**−**20**) software. Absorption correction and scaling was performed on the basis of multiple measured reflections with SADABS[45] (**14**−**16**) or SORTAV[46] (**18**−**20**). In compound **17**, no absorption correction was considered necessary. The structures were solved by Direct Methods using the SHELXS-97[47] (**14**−**17**, **19**, and **20**) or SIR-97[48] (**18**) program. Least-squares refinement was performed with SHELXL-97[47] against F^2 for all reflections. Non-hydrogen atoms were refined freely with anisotropic displacement parameters. Hydrogen atoms were introduced in calculated positions (**14**−**18** and **20**) or located in difference Fourier maps (**19**). Hydrogen atoms were refined with a riding model, and the N−H hydrogen atom of **19** was refined freely with isotropic displacement parameters. Restraints for distances and angles and for the approximation of isotropic behavior were used for triflate and acetonitrile. In **14**, **16**−**18**, and **20**, triflate anions were refined with disorder models. In **14**, the acetonitrile was refined with partial occupancy, and the propyl ester moiety, with a disorder model. The crystal structures of **15** and **20** contain voids [594 (compound **15**) and 282 $Å^3$/unit cell (compound **20**)] filled with disordered acetonitrile solvent molecules. Their contribution to the structural factors was secured by back-Fourier transformation with the SQUEEZE routine of PLATON,[49] resulting in 112 (compound **15**) and 70 electrons/unit cell (compound **20**). Geometry calculations and checking for higher symmetry was performed with the PLATON program.[49]

Further details of the crystal structure determinations are given in Tables 10−12.

DFT Geometry Optimizations. The geometry optimizations were carried out with the Turbomole program[51a,b] coupled to the PQS Baker optimizer.[52] Geometries were fully optimized as minima at the ri-DFT BP86[53] level using the Turbomole SV(P) basis set[51c,d] on all atoms. Improved energies were obtained with single-point energy calculations at the DFT b3-lyp,[54] def-TZVP[51c−f] level of theory.

Table 12. Experimental Details of the Crystal Structure for 20

	20
formula	$[C_{44}H_{72}FeN_8O_4](CF_3O_3S)_2$ + disordered acetonitrile
fw	1131.09[a]
cryst color	yellow
cryst size (mm^3)	0.26 × 0.24 × 0.06
cryst syst	triclinic
space group	*P*1 (No. 1)
a (Å)	12.7766(1)
b (Å)	13.9229(1)
c (Å)	27.2566(4)
α (deg)	80.8220(3)
β (deg)	84.8511(4)
γ (deg)	67.7105(7)
V ($Å^3$)	4426.61(8)
Z	3
D_{calc} (g/cm^3)	1.273[a]
$(\sin\theta/\lambda)_{max}$ ($Å^{-1}$)	0.65
reflns. measured/unique	88 288/39 932
parameters/restraints	2142/2229
R1/wR2 [$I > 2\sigma(I)$]	0.0496/0.1116
R1/wR2 (all reflns.)	0.0786/0.1264
S	0.999
Flack x[50]	0.537(9)
ρ(min/max) ($eÅ^{-3}$)	−0.32/0.57

[a]Derived values do not contain the contribution of the disordered solvent.

dx.doi.org/10.1021/ic400096e | Inorg. Chem. 2013, 52, 7394−7410

■ ASSOCIATED CONTENT

Supporting Information

CIF file for the X-ray crystal structures of compounds **14**–**20**. This material is available free of charge via the Internet at http://pubs.acs.org.

■ AUTHOR INFORMATION

Corresponding Author

*E-mail: r.j.m.kleingebbink@uu.nl.

Notes

The authors declare no competing financial interest.

■ ACKNOWLEDGMENTS

This work was financially supported by the National Research School Combination-Catalysis (NRSC-C).

■ REFERENCES

(1) Tanase, S.; Bouwman, E. *Adv. Inorg. Chem.* **2006**, *58*, 29–75.
(2) Bataille, C. J. R.; Donohoe, T. J. *Chem. Soc. Rev.* **2011**, *40*, 114–128.
(3) Schroeder, M. *Chem. Rev.* **1980**, *80*, 187–213.
(4) Sharpless, K. B.; Amberg, W.; Bennani, Y. L.; Crispino, G. A.; Hartung, J.; Jeong, K.-S.; Kwong, H.-L.; Morikawa, K.; Wang, Z.-M.; Xu, D.; Zhang, X.-L. *J. Org. Chem.* **1992**, *57*, 2768–2771.
(5) Yip, W.-P.; Ho, C.-M.; Zhu, N.; Lau, T.-C.; Che, C.-M. *Chem.—Asian J.* **2008**, *3*, 70–77.
(6) Shing, T. K. M.; Tam, E. K. W.; Tai, V.W.-F.; Chung, I. H. F.; Jiang, Q. *Chem.—Eur. J.* **1996**, *2*, 50–57.
(7) Yip, W.-P.; Yu, W.-Y.; Zhu, N.; Che, C.-M. *J. Am. Chem. Soc.* **2005**, *127*, 14239–14249.
(8) Zimmer, R.; Collas, M.; Czerwonka, R.; Hain, U.; Reissig, H. *Synthesis* **2008**, *2*, 237–244.
(9) Taylor, J. E. *Can. J. Chem.* **1984**, *62*, 2641–2645.
(10) de Boer, J. W.; Browne, W. R.; Harutyunyan, S. R.; Bine, L.; Tiemersma-Wegman, T. D.; Alsters, P. L.; Hage, R.; Feringa, B. L. *Chem. Commun.* **2008**, 3747–3749.
(11) Chow, T. W.-S.; Liu, Y.; Che, C.-M. *Chem. Commun.* **2011**, *47*, 11204–11206.
(12) Bruijnincx, P. C. A.; van Koten, G.; Klein Gebbink, R. J. M. *Chem. Soc. Rev.* **2008**, *37*, 2716–2744.
(13) Costas, M.; Mehn, M. P.; Jensen, M. P.; Que, L., Jr. *Chem. Rev.* **2004**, *104*, 939–986.
(14) Hegg, E. L.; Que, L., Jr. *Eur. J. Biochem.* **1997**, *250*, 625–629.
(15) Chen, K.; Que, L., Jr. *Angew. Chem., Int. Ed.* **1999**, *38*, 2227–2229.
(16) Oldenburg, P. D.; Shteinman, A. A.; Que, L., Jr. *J. Am. Chem. Soc.* **2005**, *127*, 15672–15673.
(17) Suzuki, K.; Oldenburg, P. D.; Que, L., Jr. *Angew. Chem., Int. Ed.* **2008**, *47*, 1887–1889.
(18) (a) Bukowski, M. R.; Comba, P.; Lienke, A.; Limberg, C.; de Laorden, C. L.; Mas-Ballesté, R.; Merz, M.; Que, L., Jr. *Angew. Chem., Int. Ed.* **2006**, *45*, 3446–3449. (b) Chow, T.W.-S.; Wong, E.L.-M.; Guo, Z.; Liu, Y.; Huang, J.-S.; Che, C.-M. *J. Am. Chem. Soc.* **2010**, *132*, 13229–13239.
(19) (a) Rodriguez, M.-C.; Morgenstern-Badarau, I.; Cesario, M.; Guilhem, J.; Keita, B.; Nadjo, L. *Inorg. Chem.* **1996**, *35*, 7804–7810. (b) Beck, A.; Weibert, B.; Burzlaff, N. *Eur. J. Inorg. Chem.* **2001**, 521–527. (c) Beck, A.; Barth, A.; Hübner, E.; Burzlaff, N. *Inorg. Chem.* **2003**, *42*, 7182–7188.
(20) (a) Dungan, V. J.; Wong, S. M.; Barry, S. M.; Rutledge, P. J. *Tetrahedron* **2012**, *68*, 3231–3236. (b) Paria, S.; Halder, P.; Paine, T. K. *Inorg. Chem.* **2010**, *49*, 4518–4523.
(21) Jones, M. W.; Baldwin, J. E.; Cowley, A. R.; Dilworth, J. R.; Karpov, A.; Smiljanic, N.; Thompson, A. L.; Adlington, R. M. *Dalton Trans.* **2012**, *41*, 14068–14086.
(22) Bruijnincx, P. C. A.; Lutz, M.; Spek, Hagen, W. R.; Weckhuysen, B. M.; van Koten, G.; Klein Gebbink, R. J. M. *J. Am. Chem. Soc.* **2007**, *129*, 2275–2286.
(23) Bruijnincx, P. C. A.; Buurmans, I. L. C.; Goisiewska, S.; Moelands, M. A. H.; Lutz, M.; Spek, A. L.; van Koten, G.; Klein Gebbink, R. J. M. *Chem.—Eur. J.* **2008**, *14*, 1228–1237.
(24) Other studies using this ligand family were reported by Burzlaff and Holland and co-workers. See (a) Peters, L.; Hübner, E.; Burzlaff, N. *J. Organomet. Chem.* **2005**, *690*, 2009–2016. (b) Rocks, S. S.; Brennessel, W. W.; Machonkin, T. E.; Holland, P. L. *Inorg. Chim. Acta* **2009**, *362*, 1387–1390.
(25) Bruijnincx, P. C. A.; Lutz, M.; Spek, A. L.; van Faassen, E. E.; Weckhuysen, B. M.; van Koten, G.; Klein Gebbink, R. J. M. *Eur. J. Inorg. Chem.* **2005**, 779–787.
(26) Braussaud, N.; Rüther, T.; Cavell, K. J.; Skelton, B. W.; White, A. H. *Synthesis* **2001**, *4*, 626–632.
(27) Lucas, P.; El Mehdi, N.; Ho, H. A.; Belanger, D.; Breau, L. *Synthesis* **2000**, *3*, 1253–1258.
(28) Elgafi, S.; Field, L. D.; Messerle, B. A.; Turner, P.; Hambley, T. W. *J. Organomet. Chem.* **1999**, *588*, 69–77.
(29) Suijkerbuijk, B. M. J. M.; Slagt, M. Q.; Klein Gebbink, R. J. M.; Lutz, M.; Spek, A. L.; van Koten, G. *Tetrahedron Lett.* **2002**, *43*, 6565–6568.
(30) Bruijnincx, P. C. A.; Lutz, M.; Spek, A. L.; Hagen, W. R.; Weckhuysen, B. M.; van Koten, G.; Klein Gebbink, R. J. M. *J. Am. Chem. Soc.* **2007**, *129*, 2275–2286.
(31) Hagen, K. S. *Inorg. Chem.* **2000**, *39*, 5867–5869.
(32) Bergström, P.Å.; French, R. *J. Phys. Chem.* **1995**, *99*, 12603–12611.
(33) Bénisvy, L.; Chottard, J.; Marrot, J.; Li, Y. *Eur. J. Inorg. Chem.* **2005**, 999–1002.
(34) Bénisvy, L.; Halut, S.; Donnadieu, B.; Tuchagues, J.; Chottard, J.; Li, Y. *Inorg. Chem.* **2006**, *45*, 2403–2405.
(35) Robinson, K.; Gibbs, G. V.; Ribbe, P. H. *Science* **1971**, *172*, 567–570.
(36) A recent example features a dinuclear Fe(II) complex in which one of the iron centers is found to be either six- or seven-coordinate within the crystal as the result of a coordination shift of an exogeneous carboxylate ligand. See Burger, B.; Dechert, S.; Große, C.; Demeshko, S.; Meyer, F. *Chem. Commun.* **2011**, *47*, 10428–10430.
(37) Britovsek, G. J. P.; Gibson, V. C.; Spitzmesser, S. K.; Tellmann, K. P.; White, A. J. P.; Williams, D. J. *J. Chem. Soc., Dalton Trans.* **2002**, 1159–1171.
(38) Evans, D. F. *J. Chem. Soc.* **1959**, 2003–2005.
(39) Oldenburg, P. D.; Feng, Y.; Pryjomska-Ray, I.; Ness, D.; Que, L., Jr. *J. Am. Chem. Soc.* **2010**, *132*, 17713–17723.
(40) Oldenburg, P. D.; Ke, C.-Y.; Tipton, A.; Shteinman, A. A.; Que, L., Jr. *Angew. Chem., Int. Ed.* **2006**, *45*, 7975–7978.
(41) Company, A.; Gómez, L.; Fontrodona, X.; Ribas, X.; Costas, M. *Chem.—Eur. J.* **2008**, *14*, 5727–5731.
(42) Duisenberg, A. J. M.; Kroon-Batenburg, L. M. J.; Schreurs, A. M. M. *J. Appl. Crystallogr.* **2003**, *36*, 220–229.
(43) Schreurs, A. M. M.; Xian, X.; Kroon-Batenburg, L. M. J. *J. Appl. Crystallogr.* **2010**, *43*, 70–82.
(44) Otwinowski, Z.; Minor, W. In *Methods in Enzymology*; Carter, C. W., Jr., Sweet, R. M., Eds.; Academic Press: San Diego, 1997; Vol. *276*, pp 307–326.
(45) Sheldrick, G. M. *SADABS: Area-Detector Absorption Correction*, version 2.10; Universität Göttingen: Göttingen, Germany, 1999.
(46) Blessing, R. H. *Acta Crystallogr.* **1995**, *A51*, 33–38.
(47) Sheldrick, G. M. *Acta Crystallogr.* **2008**, *A64*, 112–122.
(48) Altomare, A.; Burla, M. C.; Camalli, M.; Cascarano, G. L.; Giacovazzo, C.; Guagliardi, A.; Moliterni, A. G. G.; Polidori, G.; Spagna, R. *J. Appl. Crystallogr.* **1999**, *32*, 115–119.
(49) Spek, A. L. *Acta Crystallogr.* **2009**, *D65*, 148–155.
(50) Flack, H. D. *Acta Crystallogr.* **1983**, *A39*, 876–881.
(51) (a) Ahlrichs, R.; Bär, M.; Baron, H.-P.; Bauernschmitt, R.; Böcker, S.; Ehrig, M.; Eichkorn, K.; Elliott, S.; Furche, F.; Haase, F.; Häser, M.; Hättig, C.; Horn, H.; Huber, C.; Huniar, U.; Kattannek, M.;

Köhn, A.; Kölmel, C.; Kollwitz, M.; May, K.; Ochsenfeld, C.; Öhm, H.; Schäfer, A.; Schneider, U.; Treutler, O.; Tsereteli, K.; Unterreiner, B.; von Arnim, M.; Weigend, F.; Weis, P.; Weiss, H. *Turbomole*, version 5.8; Theoretical Chemistry Group, University of Karlsruhe: Karlsruhe, Germany, 2002. (b) Treutler, O.; Ahlrichs, R. *J. Chem. Phys.* **1995**, *102*, 346−354. (c) Turbomole basisset library, *Turbomole*, version 5.8; see a. (d) Schäfer, A.; Horn, H.; Ahlrichs, R. *J. Chem. Phys.* **1992**, *97*, 2571−2577. (e) Andrae, D.; Haeussermann, U.; Dolg, M.; Stoll, H.; Preuss, H. *Theor. Chim. Acta* **1990**, *77*, 123−141. (f) Schäfer, A.; Huber, C.; Ahlrichs, R. *J. Chem. Phys.* **1994**, *100*, 5829−5835. (g) Ahlrichs, R.; May, K. *Phys. Chem. Chem. Phys.* **2000**, *2*, 943−945.

(52) (a) *PQS*, version 2.4; Parallel Quantum Solutions: Fayetteville, AR, 2001. (The Baker optimizer is available separately from PQS upon request.) (b) Baker, J. *J. Comput. Chem.* **1986**, *7*, 385−395.

(53) (a) Becke, A. D. *Phys. Rev. A* **1988**, *38*, 3098−3100. (b) Perdew, J. P. *Phys. Rev. B* **1986**, *33*, 8822−8824.

(54) (a) Lee, C.; Yang, W.; Parr, R. G. *Phys. Rev. B* **1988**, *37*, 785−789. (b) Becke, A. D. *J. Chem. Phys.* **1993**, *98*, 1372−1377. (c) Becke, A. D. *J. Chem. Phys.* **1993**, *98*, 5648−5652. (d) Calculations were performed using the Turbomole functional b3-lyp, which is not identical to the Gaussian B3LYP functional.